NASA-CR-194117

Final Report

Submitted to:	National Aeronautics and Space Administration, Langley Research Center Hampton, VA 23665-5225. Attn: Dr. Ronald A. Outlaw Technical Office, M/S 493
Institution:	Hampton University, Department of Physics, Hampton, VA 23668.
Title of Research:	Hydrogen Partitioning and Transport in Titanium Aluminides.
NASA Grant No:	NAG-1-1110
Period Covered:	March 1,1990 - Aug 28, 1993
Principal Investigator:	Dr. Kwang S. Han
Co-Principal Investigator:	Dr. Weon S. Lee

(NASA-CR-194117) HYDROGEN PARTITIONING AND TRANSPORT IN TITANIUM ALUMINIDES Final Report, 1 Mar. 1990 - 28 Aug. 1993 (Hampton Univ.) 40 p

N94-10713

Unclas

G3/25 0182915

TABLE OF CONTENTS

SUMMARY

This report gives the final summary of the research work performed under NASA grant NAG1-1110 entitled "Hydrogen Partitioning and Transport in Titanium Aluminides" which has been performed from March 1, 1990 to Aug 28, 1993. We obtained several outstanding results as follows.

1. The Surface Variation of Ti-14Al -21Nb as a function of Temperature under Ultrahigh Vacuum Conditions.

Figure 1 presents a plot of the Auger electron intensities of O, C, Al and Ti (418 eV) normalized to Ti (387eV) as a function of temperature. It is clear from this study that the Ti-14Al-21Nb alloy surface is extremely sensitive to temperature. At 300 ^{o}C, the carbon and oxygen began to rapidly dissolve into the alloy, and at 600 ^{o}C bulk of sulfur segregated to the surface. Since the variation in the surface composition is so extensive and so different over the temperature range studied, the data suggest that there may be substantial changes in the hydrogen transport. For example, the variation of the surface composition at 250, 600 and 1000 C. Although the effect of the surface composition variation on the solubility and diffusivity of hydrogen in this alloy is not known, an unambiguous measurement of these properties will require UHV techniques, sputtering and heating capability. This is a standard practice in surface analysis but has not generally been the case in past hydrogen dissolution and transport measurements.

Figure 2 shows Auger electron spectra showing cyclic sputter cleaning of Ti-14Al-21Nb alloy to remove segregated sulfur. We suggest this technique for desulfurization to overcome a problem of the aluminum oxides scale spallation in applications of the high temperature engine materials.

Details of the surface variation of Ti-14-21Nb as a function of Temperature under Ultrahigh Vacuum conditions was published on Journal of Electrochemical Society Vol. 13, April issue, No. 4. 1194-1196(l990).

2. Titanium Aluminides: Surface Composition Effects as a Function of Temperature.

Figure 3 shows the surface variation of oxygen concentration as a function of temperature from 20 C to 1000 C for pure Ti, alpha-2 aluminide and gama aluminide. The alpha-2 and gama aluminides had the same initial oxygen concentration, but as compared with pure titanium, the oxygen seemed to decline in concentration almost immediately. The alpha-2 and gama aluminides had similar concentrations and slopes until T>700 C where a dramatic divergence in their respective concentrations was seen. The oxygen intensity for the alpha-2 continued to decline to a final level of about 10% at 1000 C, but the intensity for the gama aluminide sharply is increased to about 54% concentration at 900 C and then fell again to 34% at 1000 C. This behavior indicates that the gama aluminide surface concentration has changed in such a way that oxygen diffuses from the bulk to form aluminum oxides.

Figure 4 shows the variation of sulfur concentration as a function of temperature for the pure titanium and the alpha-2 and gama aluminides. The segregation of the sulfur to the surface appears to be strongly inhibited by the species (i.e., carbon or oxygen) interacting with titanium. For example, the three sulfur curves are almost exactly the inverse of the oxygen curves shown in figure 3, which indicates that the sulfur will not segregate until the oxygen is substantially depleted from the surface region. To a lesser extent, the same appears to be true for sulfur segregation following the carbon dissolution, since carbon closely follows the oxygen dissolution. Further, no peak shape variation or energy shift was observed for the sulfur (152eV) transition, which suggests that the sulfur surface bond is a tenuous one. The sulfur intensity increased dramatically at T>500 C for the pure titanium and somewhat slower for the alpha-2 aluminide, but since the gama aluminide retained a rather significant oxygen level at high temperature, the detected sulfur never increased beyond 10%, even at 1000 C. The sulfur was found to be easily removed from the surface, by short-term Ar ion sputtering or by in situ oxygen exposure, which further confirms that the sulfur was weakly bound.

Details of "Surface Composition Effects as a Function of Temperature" will be found in Journal of Scripta Metallugica et Materialia" Vol.24, pp171-176 (l990). Appendix 1.

3. Auger Electron Intensity Variation in Oxygen-Charged Silver

Figure 5 shows a tracing of the grain structure in the region studied which are the (421) and (221) grains. The (221) grain is only about 15 degree off of the (111) pole. The grain boundary at the top of the tracing is probably a tilt or twist boundary. The (421) grain appears to be rotated about 90 degree from the [110] direction of the (221). The angle between the poles of these two orientations was approximately 19 degree.

Figure 6 shows Auger images and line scans of silver and oxygen after a brief cleaning by Ar ion bombardment (Figs. 6a and 6b) and after a subsequent anneal at 470 C in UHV for 30 minutes (Figs. 6c and 6d). Figure 6b, however, which represents the dissolved oxygen image and line scan, does not show any significant contrast. After heating the sample at 470 C in UHV for 30 minutes, the damage incurred by ion bombardment was annealed out, and the contrast shown in figure 6c was correspondingly greater. The annealing, however, did not significantly improve the dissolved oxygen contrast between the grains (fig.6d) but did appear to concentrate more oxygen at the surface. These results indicate that the observed contrast strongly depends on the surface order of the grains. The source of the contrast is quite probably the variation in the Auger electrons caused by the different directions of forward focusing in each grain. This diffraction of the outgoing electrons is primarily caused by the over lying lattice atoms to a depth of about 4 atomic layers. Multiple scattering also plays an important role in preventing intensity enhancements in the emission from deeper than the top few layers. The lack of oxygen contrast in the same two grains may be because oxygen atoms are randomly distributed throughout the Ag surface or subsurface and are not in positions aligned with chains of Ag atoms. It is assumed that most of the oxygen atoms are located in the octahedral interstitial sites of the Ag because the radius of the octahedral sites is much larger than that of the tetrahedral sites of the fcc structure, and is also comparable to the single- bond covalent radius of the oxygen atoms. These interstitial regions are also affected by surface relaxation, which occurs in the form of expansions and contractions that do not change the two-dimensional lattice but do change in the z-direction near the surface. The varying layer spacing normal to the surface exhibits a damped oscillatory size distribution. Most oxygen atoms will probably be located between the second and third layers because the spacing is generally expanded, whereas the spacing between the first and second layers is

generally contracted.

Figure 7 shows images and line scans of different Auger transition energies of silver after heating the sample at 470 C in UHV for 30 minutes. The contrast of the Auger images of silver on different grains shows a strong dependence with transition energy. The highest contrasts are shown in figs. 7a and 7e, the 356 eV and 27 eV transitions, respectively. The lowest contrast is shown Fig. 7c, the 265eV transition. Moderate contrasts are shown in figs. 7b and 7d, the 303eV and 78eV transitions, respectively. In figs. 7a-7c, it is found that the lower the Ag Auger electron energy, the less the contrast of the Auger images on different grains. The 256eV transition exhibits the least contrast and can be explained by the fact that forward focusing at this electron energy along low-index directions is limited because of multiple scattering, i.e., the Auger electron emerges without a strong preference for a particular direction.

Details of "Auger Electron Intensity Variation in Oxygen-Charged Silver" will be found on Journal of Applied Science 47 (1991)91-98. (Appendix 2).

4. Segregation of Sulfur on a Titanium Surface Studied by Auger Electron Spectroscopy

Figure 8 shows the variation of the sulfur, carbon, titanium and oxygen Auger peaks normalized to the titanium (383eV) peak as a function of temperature. The data at each temperature represent an average of several measurements taken at three or more locations. Above 200 ^{o}C the oxygen level is decreased rapidly and completely disappeared at above 600 C. The carbon level on the surface increased conversely from room temperature to 300 C and then is decreased rapidly and disappeared completely at above 500 ^{o}C. The line shape of the carbon Auger spectra was representative of molecular carbon upto 200 ^{o}C, mixtures molecular and carbidic carbon at 300 C and entirely carbidic carbon above 300 ^{o}C. The sulfur on the surface increased rapidly at above 350 ^{o}C whenever carbon and oxygen are decreased considerably. The Ti double peaks at 412 eV and 418 eV appeared a single peak at 418 eV and Ti single peak at 383 eV appeared double peak at 383 eV and 387 eV at above 300 ^{o}C. The Ti (418 eV) peak increased rapidly at 400 C and then saturated at above 500 ^{o}C. At this temperature oxygen and carbon were not significant but

sulfur was considerably segregated on the surface. From this experiment We ascertained that intensity of the Ti (418 eV) peak is not affected by the amount of surface sulfur segregated from the bulk, but only affected by the amount of surface oxygen and carbon.

Figure 9 illustrates the variation of the sulfur Auger peak normalized to the titanium 383 eV peak as a function of time at the different temperature. These S/Ti ratios were used rather than the absolute Auger peak-to-peak height (APPH) for sulfur to eliminate sensitivity changes resulting from change in operating conditions during the measurements.
These segregation experiments were performed by recording Auger spectra as a function of time and temperature after sputtering 400 ^{0}C to minimized the desulfurization. These curves give information relating the segregation of sulfur in titanium. For the case where sulfur buildup on the sample surface is controlled by the diffusion of sulfur to the surface, the amount of surface sulfur should be proportional to the square root of the annealing time.

Figure 10 shows the variation of the sulfur Auger peak normalized to the titanium (383 eV) peak as a function of the square root of the annealing time at the different temperatures. As shown in figure 10, such a proportionality existed for 450, 500, and 550 ^{0}C curves between approximately 2 and 8 minutes., but for 600 and 650 ^{0}C curves very short time intervals. The average slopes of the curves in this region can be taken as the rate (Ri) of sulfur segregation on the surface. The resulting rates are tabulated in Table I. In order to achieve some understanding of the mechanism for sulfur segregation, an Arrhenius analysis of the data was made. By plotting log Ri vs 1/T (1/K), the activation energy (Ea) can be estimated from the Arrhenius relationship.

Figure 11 shows the Arrhenius plot for sulfur segregation in titanium. Note the distinct linearity of the plot. From Arrhenius relationship, the slope of the line equals Ea/2.3R. The activation energy, Ea,for sulfur segregation calculated from the slope of this plot is 35.8 kcal/mole. This value is not consistent with previous study by Khan. He performed the segregation experiment in Ti single crystal by recording Auger spectra as a function of time and temperature after sputter cleaning at 720 ^{0}C and cooling down, and calculated the activation energy, Ea= 21.18 kcal/mole, from the slope of Arrhenius plot composed by only

three data points. As shown in figure 2, the amount of surface sulfur segregated from the bulk are evidently decreased by cyclic sputter cleaning at very high temperature. This result indicates that the values of the activation energy may be affected by the sputter cleaning temperature or bulk impurity levels. However, Leygraf and Ekelund found that sulfur segregation at 425 C more rapid on single crystal iron samples than on polycrystalline iron samples. Since single crystal samples have no grain boundaries, the sulfur segregation observed by Leygraf and Ekelund at 425 ^{0}C was not due to sulfur diffusing to the surface in grain boundaries. Because of this potentially contradictory information, it is not certain what type of diffusion the 35.8 kcal/mole activation energy represents.

Figure 12 shows the variation of the sulfur Auger peaks normalized titanium (383 eV) peak as a function of sputtering time at 400 ^{0}C. The intensity of the Ti (418 eV) Auger peak is almost constant between as the amount of the surface sulfur is maximized by the segregation at 800 ^{0}C for 2hrs and as surface sulfur is completely removed by Ar ion sputtering. This indicates that the segregated sulfur on the titanium does not form sulfide and is weakly bound. Since sulfur does not segregate to the surface until oxygen and carbon are substantially depleted from the surface region, We may expect that in case of the aluminum oxide coated on the titanium surface, aluminum oxide scale spallation can occur due to sulfur segregation and weakening at the aluminum oxide titanium interface.

Details of "Segregation of Sulfur on a Titanium Surface Studied by Auger Electron Spectroscopy" will be published on Journal of Applied Surface Science (l993).

List of Figures

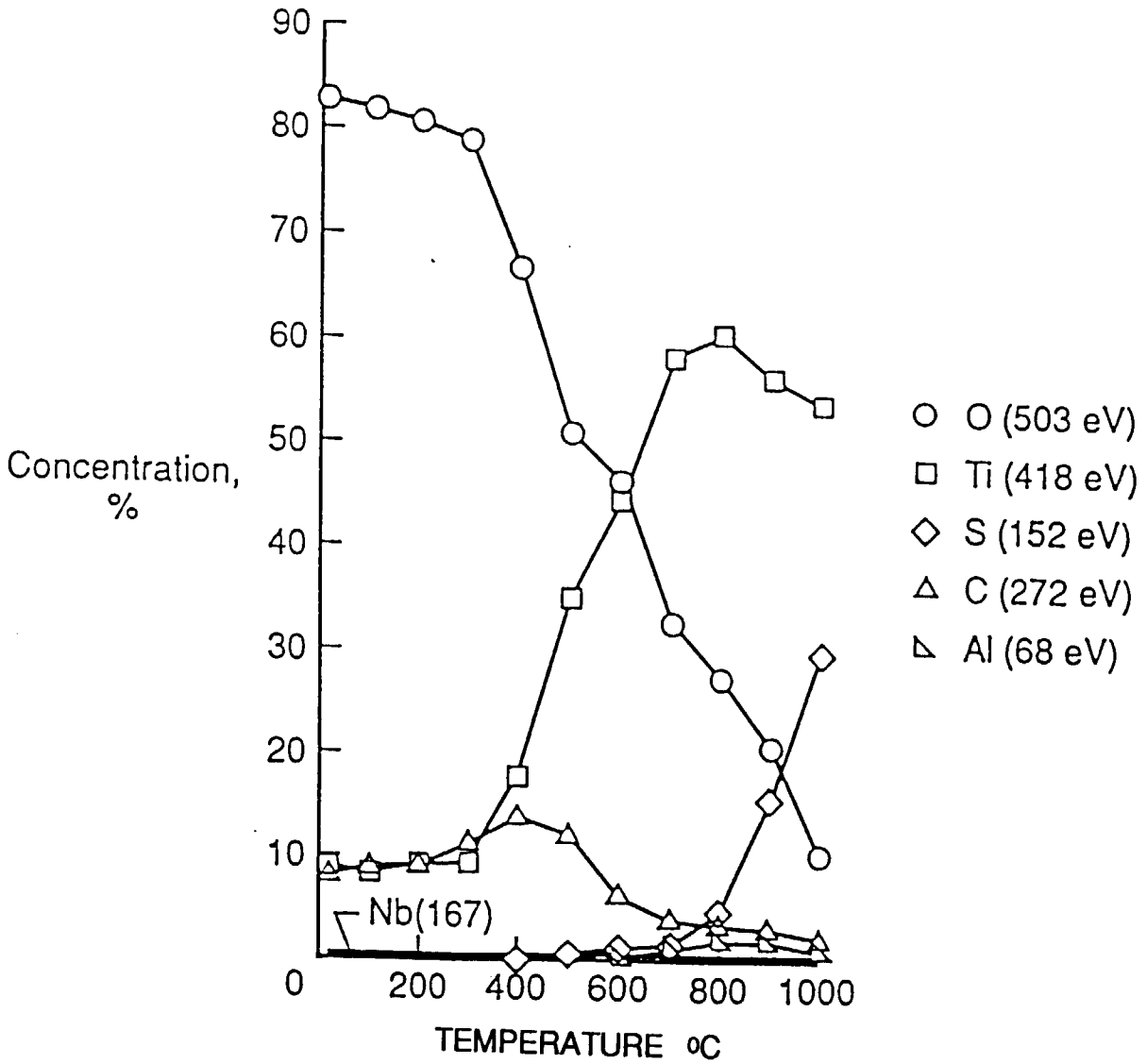

Fig. 1 Auger electron intensities of oxygen, carbon, aluminum and titanium (418 eV) normalized to Titanium (387 eV) as a function of temperature.

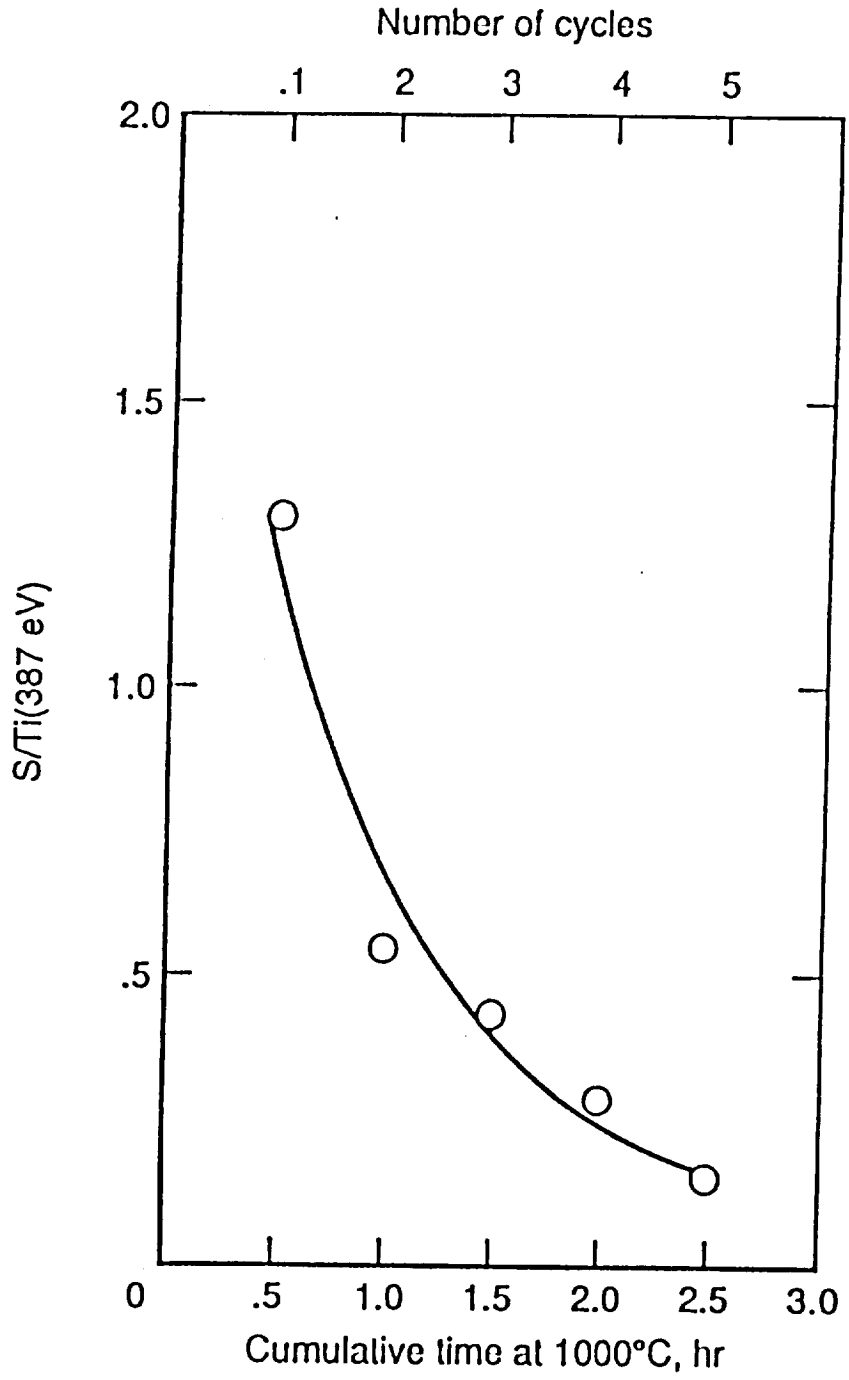

Fig. 2 Auger electron spectra showing cyclic sputter cleaning of Ti-14Al-21Nb alloy to remove segregated sulfur.

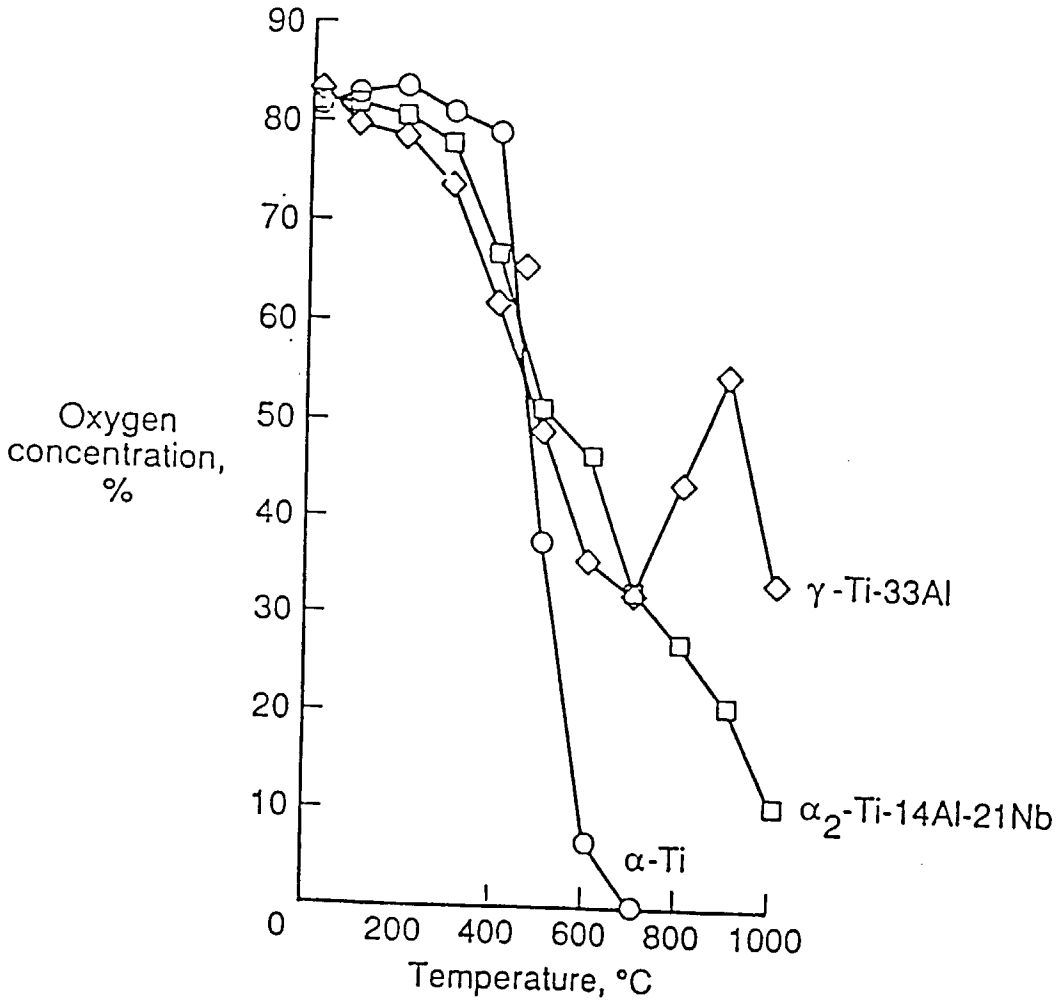

Fig. 3 Surface variation of oxygen concentration as a function of temperature.

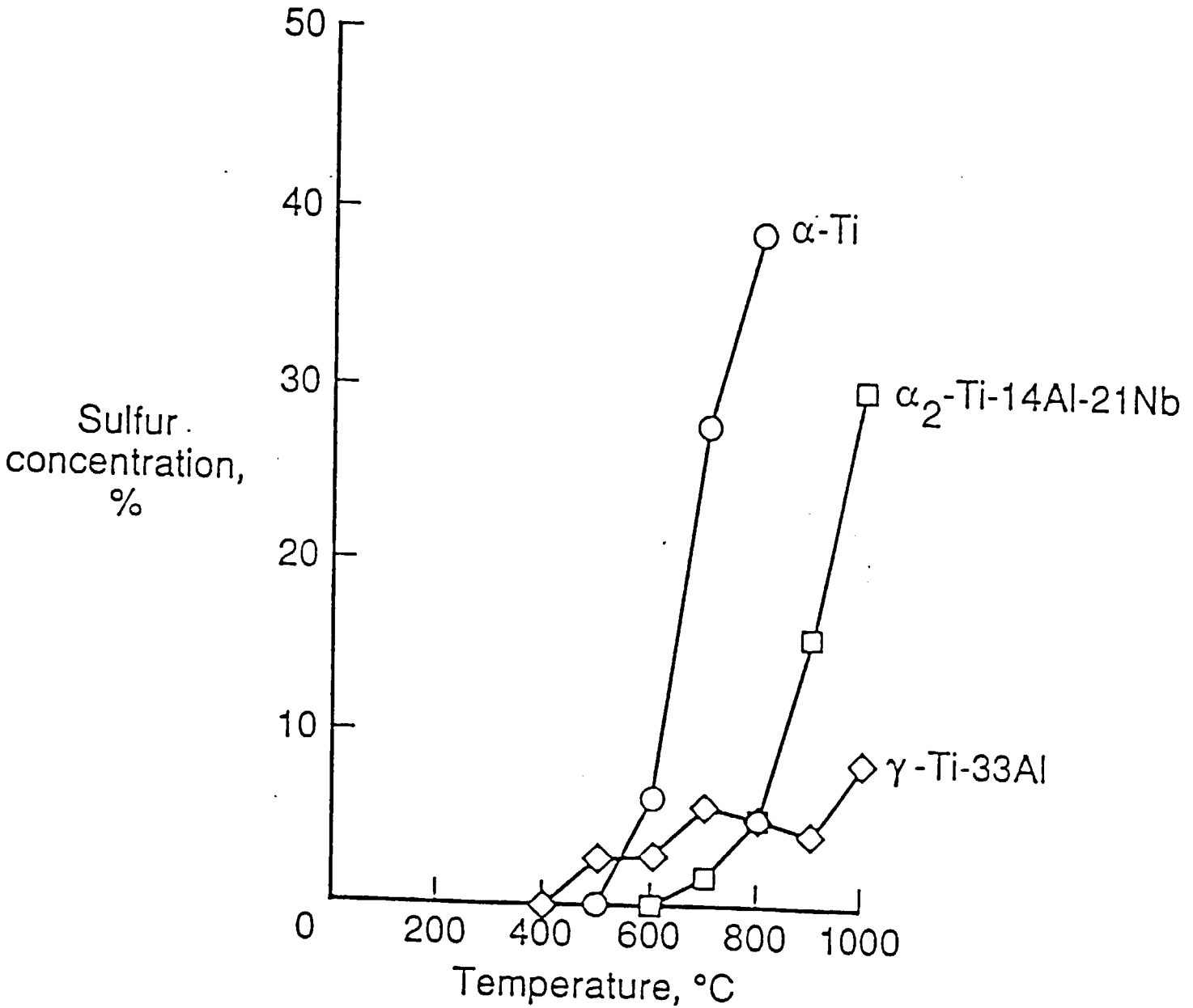

Fig. 4 Variation of sulfur concentration as a function of temperature.

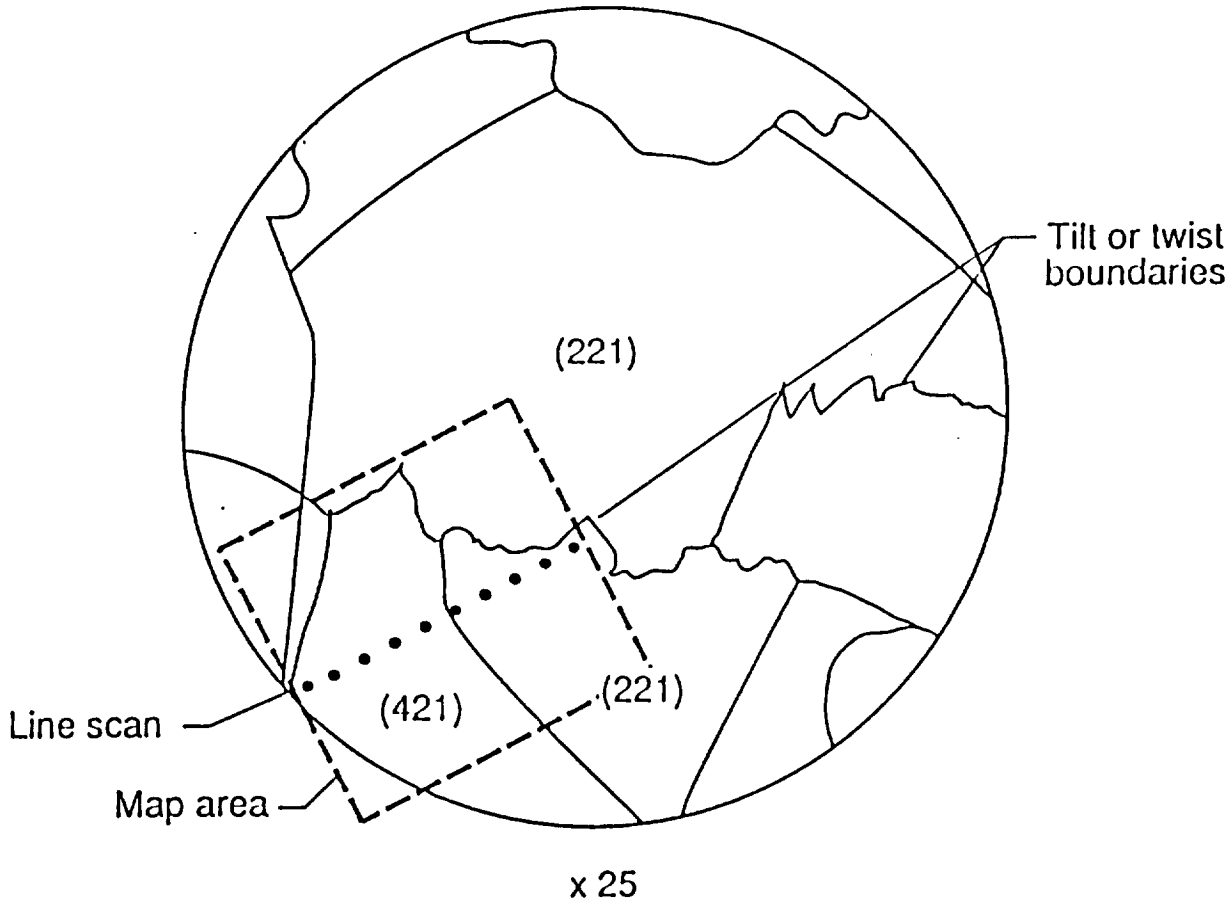

Fig. 5 The tracing of grain structure for the oxygen charged silver.

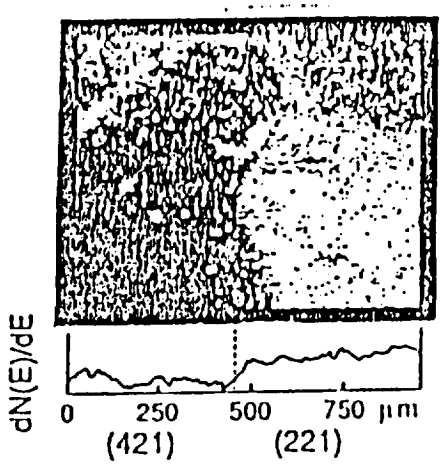

(a) Ag $M_{4,5}VV$ (356 eV).

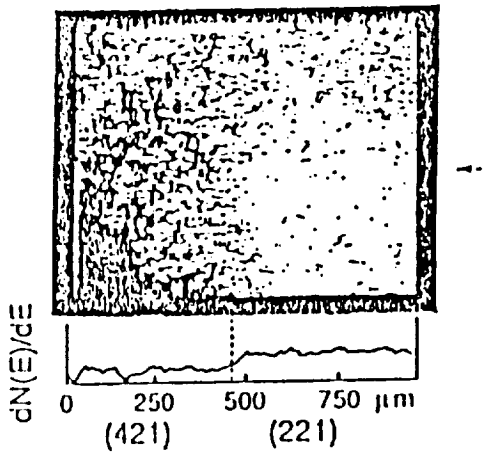

(b) Ag $M_{4,5}N_{2,3}V$ (303 eV).

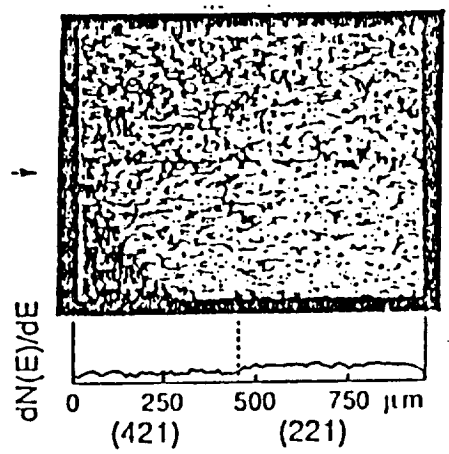

(c) Ag $M_{4,5}N_1V$ (265 eV).

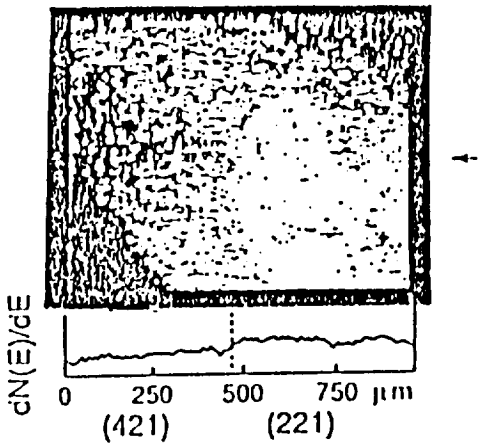

(d) Ag N_1VV (78 eV).

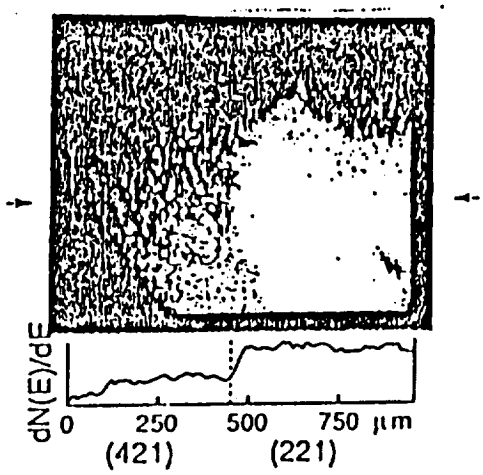

(e) Ag $N_1N_{2,3}V$ (27 eV).

Fig. 6 Auger image and line scans of silver and oxygen after a brief cleaning by argon ion bombardment.

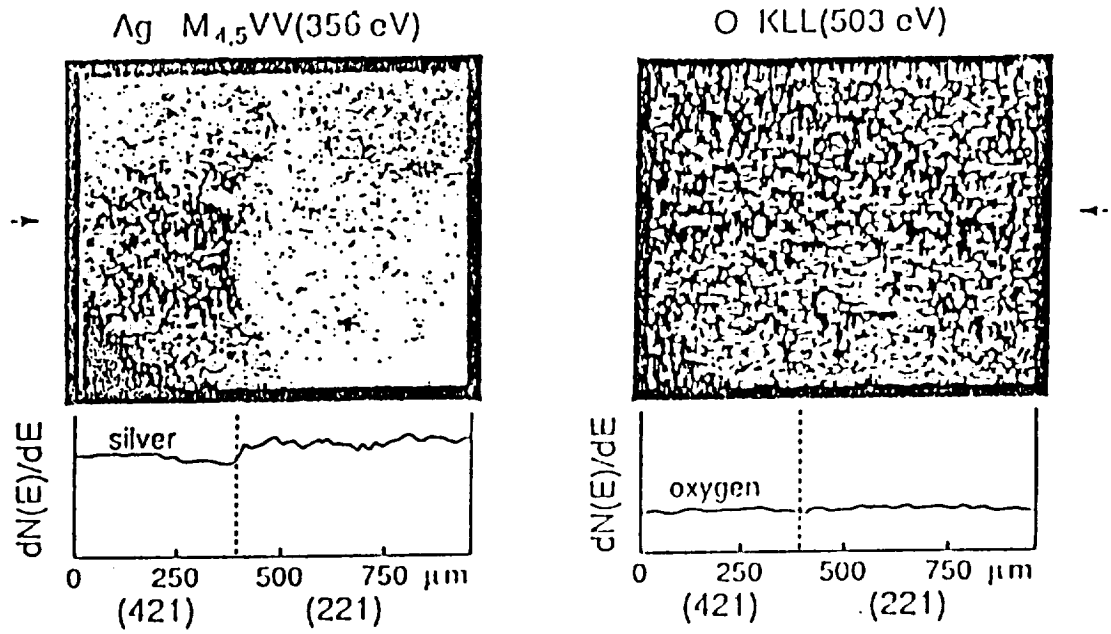

(a) Ag $M_{4,5}$VV after cleaning by ion bombardment.

(b) O KLL after cleaning by ion bombardment.

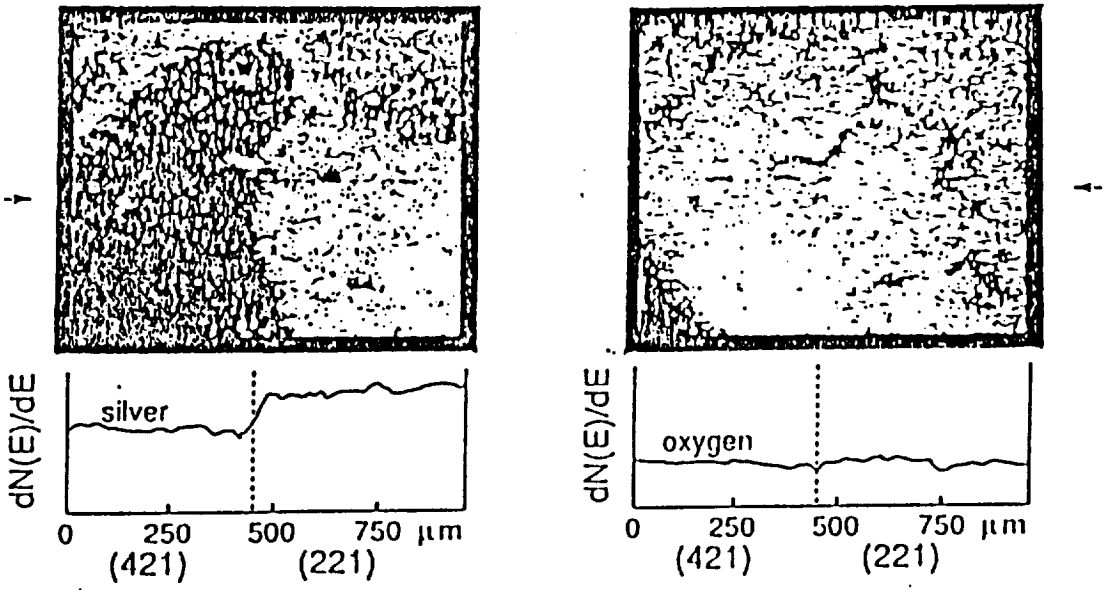

(c) Ag $M_{4,5}$VV after heating at 470° C in UHV for 30 min.

(d) O KLL after heating at 470° C in UHV for 30 min.

Fig. 7 Images and line scans of a different Auger transition energy of silver after heating the sample at 470°C in UHV for 30 minutes.

Variation of the sulfur, carbon, titanium and oxygen Auger peak normalized to the titanium (383 eV) peak as a function of temperature.

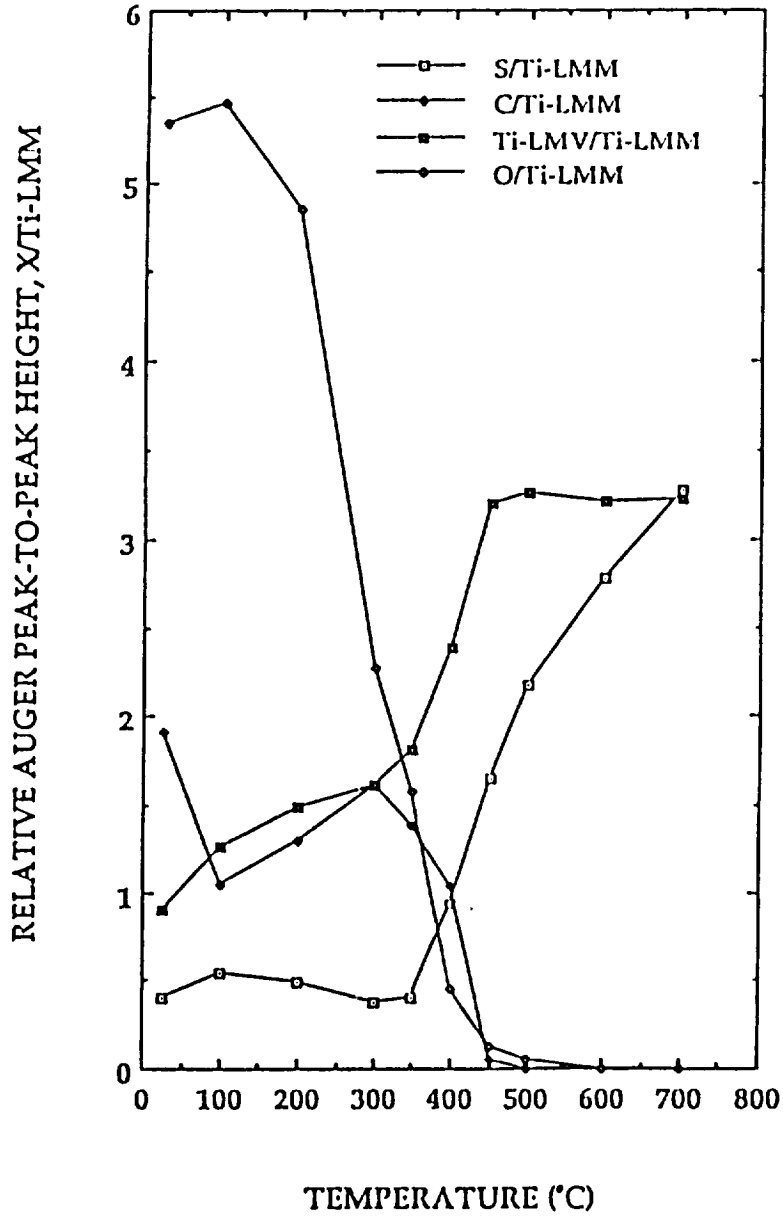

Fig. 8 Variation of the sulfur, carbon, titanium and oxygen Auger peak normalized (383 eV) peak as a function of temperature.

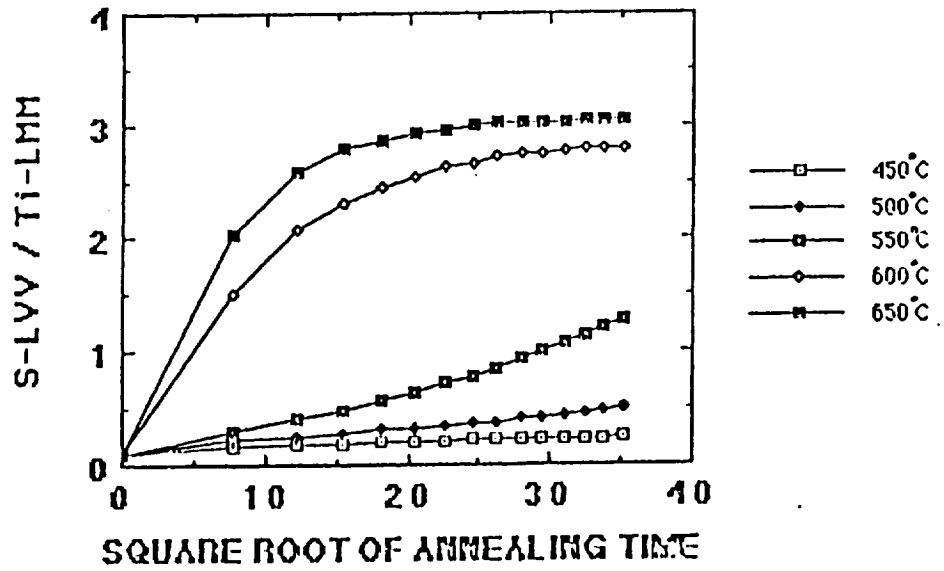

Variation of the sulfur Auger peak nomalized to the titanium (383 eV) peak as a function of the square root of the time at the different temperatures.

Fig. 9 Variation of the sulfur Auger peak normalized to the titanium (383 eV) peak as a function of time at the different temperatures.

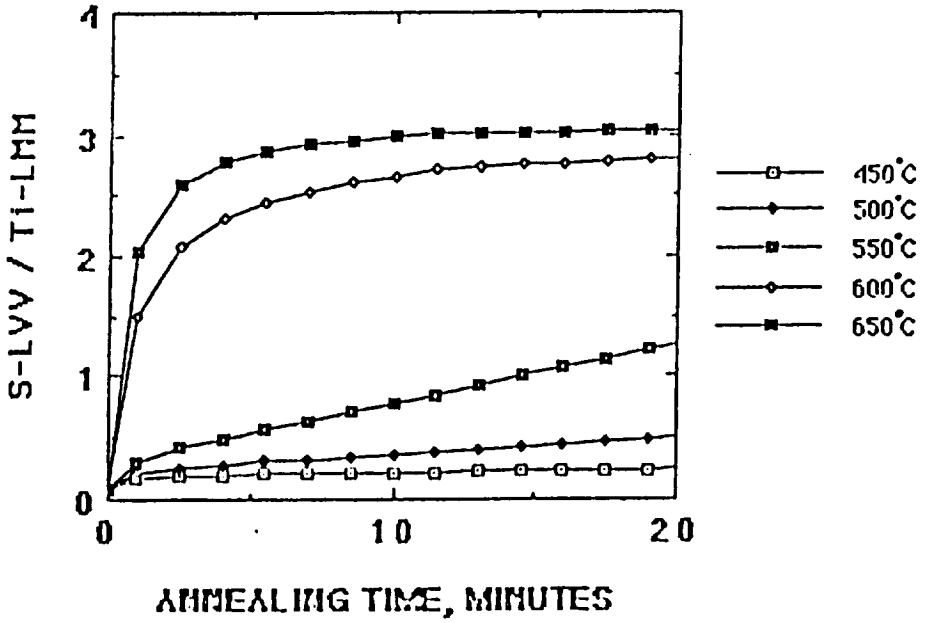

Variation of the sulfur Auger peak nomalized to the titanium (383 eV) peak as a function of time at the different temperatures.

Fig. 10 Variation of the sulfur Auger peak normalized to the titanium (383eV) peak as a function of the square root of the times at the different temperatures.

Ea = 35.8 kcal/mole

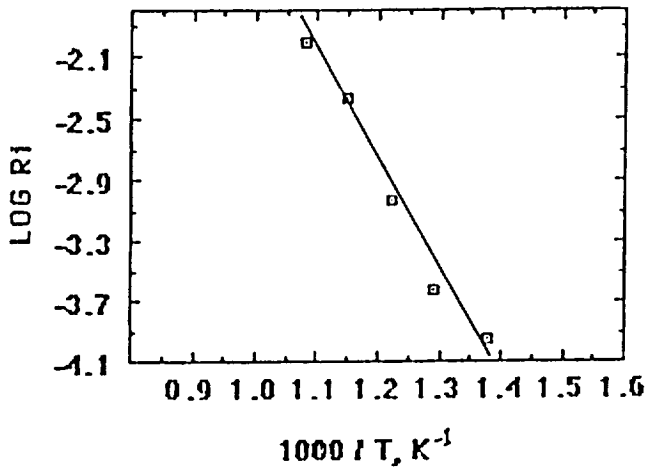

Arrhenius plot sulfur segregation data

Fig. 11 Arrenius plot of sulfur segregation data.

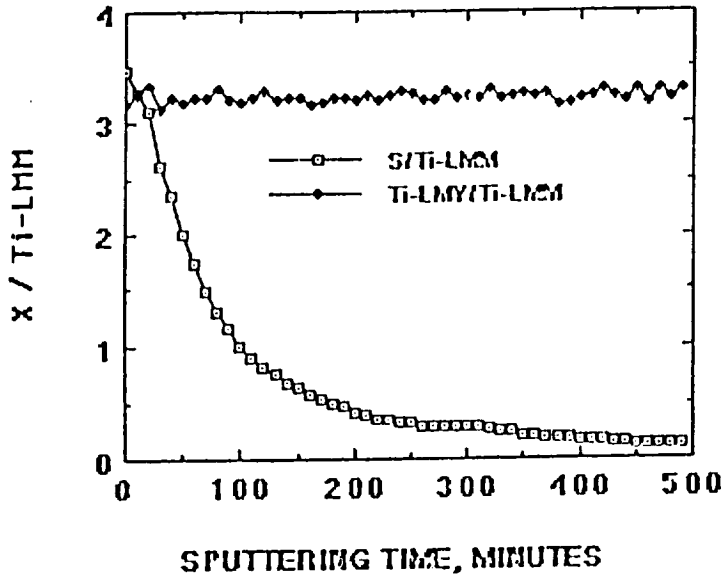

Fig. 12 Variation of the sulfur Auger peak normalized to the titanium (383 eV) peak as a function of sputtering time at 400°C (Ion current = 5nA and beam diameter = 5mm.

TABLE I, RATES OF SULFUR SEGREGATION

Temperature (°C)	Ri (Arbitrary units)
450	0.000111
500	0.000232
550	0.000933
600	0.00433
650	0.00976

List of Publication
generated
under NASA grant NAG1-1110
period March 1, 1990-Aug 28, 1993

1. W. S. Lee, S. N. Sankaran, R. A. Outlaw and R. K. Clark, The Surface Variation of Ti-14Al-21Nb as a Function of Temperature under Ultrahigh Vacuum Conditions, J. Electrochem. Soc., Vol. 137, No. 4, April (1990) pp. 1194-1196

2. W. S. Lee, R. A. Outlaw, S. N. Sankaran, R. K. Clark and D. Wu, Titanium-Aluminides: Surface Variations as a Function of Temperature, 4th NASA Review and Workshop on Hydrogen-Materials Interactions, Scottsdale, AZ, May 30-June 1, 1990

3. W. S. Lee, R. A. Outlaw, G. B. Hoflund and M. R. Davidson, Auger Electron Intensity Variations in Oxygen-Charged Silver, Appl. Surf. Sci., Vol. 47 (1991) pp. 91-98

4. R. A. Outlaw, W. S. Lee, S. N. Sankaran, D. Wu and R. K. Clark, Titanium Aluminides: Surface Composition Effects as a Function of Temperature, Scripta Metallugica, Vol. 24 (1991) pp. 171-176

5. R. A. Outlaw, W.S. Lee, S. J. Hoekje and S. N. Sankaran, "Segregation of Sulfur in Titanium Surface Selected Alloys" will be published in Journal of Applied Surface Science (1993)

Reprinted from JOURNAL OF THE ELECTROCHEMICAL SOCIETY
Vol. 137, No. 4, April 1990
Printed in U.S.A.

The Surface Variation of Ti-14Al-21Nb as a Function of Temperature Under Ultrahigh Vacuum Conditions

W. S. Lee

Department of Physics, Hampton University, Hampton, Virginia 23668

S. N. Sankaran*

Analytical Services and Materials, Incorporated, Hampton, Virginia 23666

R. A. Outlaw and R. K. Clark

NASA Langley Research Center, Hampton, Virginia 23665

Titanium aluminide intermetallic alloys are being considered for engine and structural applications in hydrogen-fueled hypersonic flight vehicles because of their low weight and high-temperature mechanical properties. During hypersonic flight, aerothermodynamic heating is so severe that parts of the vehicle need to be actively cooled by pumping hydrogen through heat exchangers at the surface.

The Ti-14Al-21Nb weight percent (w/o) alloy is a ductile modification of the intermetallic Ti_3Al to which Nb has been added to stabilize the β phase, retard ordering kinetics, and reduce planarity of slip, all of which lead to improved room temperature ductility (1-4). The known embrittling effects of hydrogen on conventional titanium alloys suggest that similar deleterious effects may be present during exposure of Ti-14Al-21Nb alloy to hydrogen. In particular, the high-temperature transport properties, such as permeability, diffusivity, and solubility of hydrogen in the alloy need to be measured, since they determine the extent of potential damage to the alloy by hydrogen.

Since titanium and its alloys chemically react with ambient gases so readily, the surface is a major factor in the transport of hydrogen in these materials. Continual chemisorption of oxygen, carbon, and nitrogen from the background environment forms sufficiently thick surface barriers (oxides, carbides, nitrides) that transport is substantially inhibited. The application of ultrahigh vacuum (UHV) conditions lessens the availability of the gaseous species and therefore lessens the barrier growth rate, but at low temperatures (<600°C), this is still the dominant mechanism. At higher temperatures (>600°C), the high solubility of titanium alloys for these gases (5-14) creates a competitive mechanism for dissolution of the barrier species into the bulk. The dissolution process is bulk diffusion-limited but clearly becomes the dominant mechanism at high temperatures and effectively removes the surface barrier. Further, dissolution has been used in the past to produce titanium alloys with known amounts of oxygen (8, 15, 16) and to produce clean surfaces during Auger electron spectroscopy (AES) studies (17). It is, therefore, essential that the surface layer first be identified and

* Electrochemical Society Active Member.

then ultimately characterized as a function of temperature in terms of its effect on hydrogen dissolution and transport in the bulk.

Experimental

The Ti-14Al-21Nb specimen for this study was machined from a hot-rolled plate material and ground with silicon carbide papers (240 grit to 1200 grit). A stable microstructure composed of predominantly equiaxed α_2 grains that would not significantly change during the subsequent lower temperature exposures was obtained by employing a homogenization heat-treatment at 1100°C [believed to be in the $\alpha_2 + \beta$ field (4)] for 1.5h in a UHV furnace. This heat-treatment resulted in a final microstructure consisting of a predominantly equiaxed α_2 matrix with small amounts of an orthorhombic phase and β phase at the triple points and grain boundaries as described by Banerjee *et al.* (4). The final sample was a square coupon, 0.5 × 0.5 × 0.05 cm in size. Just prior to introduction into the AES system, the alloy was given a standard cleaning treatment consisting of: ultrasonic cleaning for 10-20 min in laboratory detergent solution; rinsing in deionized water and methanol; acid cleaning until bright (usually for less than a minute) in a solution of 30% HNO_3, 2% HF and 68% deionized water maintained at ≈54°C; rinsing in deionized water and methanol; and finally, thorough drying in hot air.

Figure 1a shows the AES spectrum of the alloy surface (predominantly the α_2 microstructure) in the as-prepared condition. The AES data were obtained with a cylindrical mirror analyzer (CMA) operated with a 10 kV coaxial gun at an energy of 3 keV and a beam current of 1 μA. The base pressure in the system was approximately 2×10^{-11} torr. The spectrum shows substantial amounts of carbon and oxygen on the surface which are characteristic of the gettering of atmospheric gases by the sample prior to introduction into the AES system. Although the titanium Auger transitions, such as the LMV shake up (387 eV) (18), the LMV (418 eV), and the LVV (451 eV) are prominent, the aluminum LVV (67 eV) and the interatomic transition Al (L_1) O ($L_{2,3}L_{2,3}$) (49 eV) (19) are also detectable. Comparing the spectrum of Fig. 1a to that reported by Solomon and Baun (19), it appears that the O to Ti peak ratios correspond to TiO_2. After the initial characterization of the surface, the sample was heated *in situ* using a heater assembly described previously (20).

Results and Discussion

After heating to 1000°C in 100°C increments, the spectrum shown in Fig. 1b was obtained. The carbon and oxygen were apparently incorporated into the bulk and sulfur was segregated to the surface. The aluminum and niobium signals (with short inelastic mean-free paths) are now quite

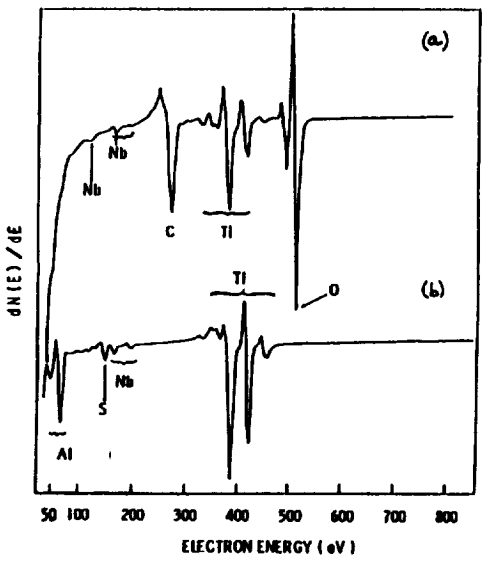

Fig. 1. (a) AES spectrum of as-received Ti-14Al-21Nb. (b) AES spectrum after heating to 1000°C in UHV environment ($p \sim 10^{-11}$ torr).

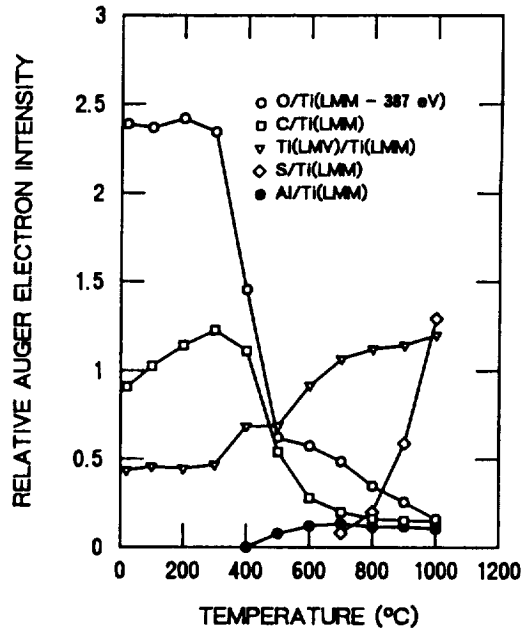

Fig. 2. Changing surface composition as a function of temperature (time at each temperature was 30 min).

prominent. Figure 2 presents a plot of the Auger electron intensities of O, C, S, Al, and Ti (418 eV) normalized to Ti (387 eV) as a function of specimen exposure temperature. The exposures were for ≈30 min, and spectra were taken at the experiment temperature and after cooling the sample to room temperature. The data at each temperature represent an average of several measurements taken at three or more locations. Although an induced current image was used to view the sample surface, this image did not have adequate resolution to reveal the detailed microstructure of the sample. However, the data between several locations did not show any significant variation, leading us to believe that all analyses were on the α_2 phase. As is evident, C and O on the surface decreased rapidly at sample temperatures exceeding 300°C, and dropped to negligible levels at about 1000°C, reflecting dissolution into the bulk. The behavior of the Ti (418 eV) peak ratio, *i.e.*, Ti (418)/Ti (387) changes from ≈0.45 in the as-prepared condition to ≈1.2 after heating to 1000°C. As described by Pons *et al.* (21), the peak at 418 eV (LMV) arises from the Ti valence electron, and its amplitude is strongly dependent on the binding forces with other surface atoms. Thus, this ratio is far less than 1.0 when the Ti surface is contaminated with C and O and exceeds 1.0 when a pure titanium surface is examined. The saturation of the Ti (418 eV) peak ratio to a value ≈1.2 as shown in Fig. 2 and a reduction in C and O peaks to very low levels indicate that the metal surface has been substantially cleaned of these species. Once the sample was cooled to room temperature, however, the C and O peaks steadily increased with time consistent with gettering by the surface of the CO species in the vacuum, even though the CO partial pressure was less than 5×10^{-11} torr.

A significant feature of the high-temperature UHV exposure is the appearance of the S peak of increasing intensity with temperatures above 600°C. It is obvious that high-temperature exposure has promoted the segregation of S to the surface in the present alloy in much the same manner as in unalloyed titanium (17, 21) and in stainless steel (22). It is interesting to note that the accumulation of S occurs after a substantial reduction in the C and O, suggesting that free surface sites have become available to accommodate the emerging S. Further, it appears that the S is only weakly bound to the titanium. If S were strongly bound to the Ti ($-\Delta H_f(TiS_2) \sim 80$ kcal/mol), it would result in a decrease in intensity of the Ti (LMV) valence transition at 418 eV, since the valence electrons would be tied up with the sulfur. As is apparent, the 418 eV peak is slightly

Table I. Comparison of the bulk composition and the clean surface composition

Element	Bulk composition of the sample (atomic percent)[a]	Composition of the sample surface at 1000°C (atomic percent)[b]
Al	25	10.8
Nb	11	1.1
Ti	64	82.3
S	0	5.7

[a] Chemical analysis.
[b] AES analysis.

increasing during this rapid increase of the S with temperature (Fig. 2). An interesting aspect of the segregation of S to the surface is its possible effect on the permeability of hydrogen through the alloy. Although this effect on Ti alloys is not known, it has been reported that S does reduce the permeability of hydrogen through palladium (23).

Only five cycles of sputtering and heating (1000°C for 30 min) of the sample were required to substantially decrease the S concentration in the bulk. An estimate of the sulfur concentration in the bulk was found to be about 1 ppm. Table I shows the compositional differences of the surface after heating and sputtering, compared to the bulk alloy composition. The aluminum and the niobium at the surface are substantially reduced from their bulk concentrations, leaving a predominantly titanium surface with a small sulfur contamination.

Conclusions

It is clear from this study that the Ti-14Al-21Nb alloy surface is extremely sensitive to temperature. At 300°C, the C and O began to rapidly dissolve into the alloy, and at 600°C bulk S segregated to the surface. The variation in the surface composition is so extensive and so different over the temperature range studied that the data suggest there may be substantial changes in the hydrogen transport. Note, for example, the surface composition at 250°, 600°, and 1000°C. Although the effect of the surface composition variation on the solubility and diffusivity of hydrogen in this alloy is not known, an unambiguous measurement of these properties will require UHV techniques, sputtering, and heating capability. This is a standard practice in surface analysis but has not generally been the case in past hydrogen dissolution and transport measurements.

Manuscript submitted May 30, 1989; revised manuscript received Sept. 30, 1989.

NASA Langley Research Center assisted in meeting the publication costs of this article.

REFERENCES

1. S. M. L. Sastry and H. A. Lipsitt, *Met. Trans. A*, **8A**, 1543 (1977).
2. R. Strychor, J. C. Williams, and W. A. Soffa, *Met. Trans. A*, **19A**, 225 (1988).
3. S. M. L. Sastry, "Proceedings of the Second Workshop of Hydrogen-Materials Interactions," H. G. Nelson, Editor, p. 93, NASP Program Office, Wright-Patterson AFB, Dayton, Ohio (1988).
4. D. Banerjee, A. K. Gogia, T. K. Nandi, and V. A. Joshi, *Acta Metall.*, **36**, 871 (1988).
5. A. E. Jenkins, *J. Inst. Metals*, **82**, 213 (1953-1954).
6. T. Hurlen, *ibid.*, **89m**, 128 (1960-1961).
7. M. Hansen, "Constitution of Binary Alloys," 2nd ed., p. 1069, McGraw-Hill Book Company, New York (1958).
8. K. E. Wiedemann, R. N. Shenoy, and J. Unnam, *Met. Trans. A*, **18A**, 1503 (1987).
9. P. Kofstad, P. B. Anderson, and O. J. Krudtaa, *J. Less Common Met.*, **3**, 89 (1961).
10. K. E. Wiedemann, M.S. Thesis, Virginia Polytechnic Institute and State University (1983).
11. S. N. Sankaran, R. K. Clark, J. Unnam, and K. E. Wiedemann, NASP CR-1070, Jan. 1990.
12. E. A. Gulbransen and K. F. Andrew, *Trans. AIME*, **185**, 741 (1949).
13. R. J. Waselewski and G. L. Kehl, *J. Inst. Metals*, **83**, 94 (1954-1955).
14. N. R. McDonald and G. R. Wallwork, *Oxid. Met.*, **2**, 263 (1970).
15. R. N. Shenoy, J. Unnam, and R. K. Clark, *ibid.*, **26**, 105 (1986).
16. J. Unnam, R. N. Shenoy, and R. K. Clark, *ibid.*, **26**, 231 (1986).
17. H. E. Bishop, J. C. Riviere, and J. P. Coad, *Surf. Sci.*, **24**, 1 (1971).
18. S. Mroczkowski and D. Lichtman, *J. Vac. Sci. Technol. A.*, **3**, 1860 (1985).
19. J. S. Solomon and W. L. Baun, *Surf. Sci.*, **51**, 228 (1975).
20. R. A. Outlaw and B. T. Baugh, *J. Vac. Sci. Technol.*, **21**, 1037 (1982).
21. F. Pons, J. Le Hericy, and J. P. Langeron, *Surf. Sci.*, **69**, 547 (1977).
22. R. A. Outlaw and D. T. Peterson, *Met. Trans. A.*, **14A**, 1869 (1983).
23. R. Lalauze, P. Gillard, and C. Pijolat, *J. Less Common Met.*, **138**, 179 (1988).

Scripta METALLURGICA et MATERIALIA Vol. 24, pp. 171-176, 1990 Printed in the U.S.A. Pergamon Press plc

TITANIUM ALUMINIDES: SURFACE COMPOSITION EFFECTS AS A FUNCTION OF TEMPERATURE

R. A. Outlaw, W. S. Lee,* S. N. Sankaran,** D. Wu*** and R. K. Clark
NASA Langley Research Center
Hampton, Virginia 23665-5225

(Received September 11, 1990)
(Revised October 29, 1990)

Introduction

Ordered intermetallic compounds, such as titanium aluminides, are being considered for use in hydrogen-fueled, hypersonic-flight vehicles because of their outstanding properties: high strength-to-weight ratio, high elastic modulus, and high temperature creep rupture strength (1). However, titanium aluminides, such as Ti_3Al and TiAl, have some distinct limitations, such as a lack of room temperature ductility, poor oxidation resistance, and a susceptibility to hydride formation (1, 2). Niobium is often added as a β stabilizer, since it increases the nonbasal slip activity in Ti_3Al, and the ordering behavior of the β phase is likely to influence the ductility of Ti_3Al-Nb alloy (3, 4). Furthermore, tantalum and niobium have been shown to enhance oxidation resistance (5).

The surfaces of these aluminides vary significantly with temperature, even under ultrahigh vacuum (UHV) conditions, and have been shown to have a correspondingly significant effect on the transport of hydrogen in and through these materials (6, 7). Background pressures of carbon and oxygen-bearing gases as low as 10^{-8} Pa are noticeably chemisorbed and contribute to a continually increasing oxide and carbide layer. At temperatures above ~ 650° C, a competing rate of carbon and oxygen dissolution into the bulk can dominate the barrier growth rate and actually remove these species from the surface. Clearly, this is a sensitive function of the environmental pressures and temperatures involved (7). Since it is important to establish the surface composition of these materials and their variation with temperature in order to ultimately correlate the role of surface layers as barriers to hydrogen transport, the purpose of this paper is to present results of an Auger Electron Spectroscopy (AES) study of the surfaces of pure Ti, Ti-14Al-21Nb (α_2 aluminide) and Ti-33Al-6Nb-1.4 Ta (γ aluminide) over the temperature range of 20-1000° C and under UHV conditions. The observed variations in surface composition were found to be quite dramatic and primarily indicated that the amount of retained oxygen and carbon on the surface is directly related to the quantity of aluminum in the vicinity of the surface.

*Hampton University, Hampton, Virginia 23668
**Analytical Services and Materials, Hampton, Virginia 23666
***Old Dominion University, Norfolk, Virginia 23508

0036-9748/90 $3.00 + .00

Experimental

The samples used in this work were fabricated in the shape of a 5-mm square, 0.2-mm-thick wafer. The microstructure of the pure Ti was equiaxed α grains, that of the α_2 aluminide was equiaxed α_2 grains with small amounts (10 percent) of an orthorhombic and β phase located at the grain boundaries (8), and that of the γ aluminide was γ grains (> 90 percent) with a fine dispersion of a complex second phase within the γ aluminide that was basically a tetrahedral structure. Prior to introduction into the surface analysis system, the samples were sequentially degreased and chemically cleaned (25 percent HNO_3, 2 percent HF), rinsed several times in deionized water, and hot-air dried. The AES data were obtained with a cylindrical mirror analyzer (CMA) operated with a 10 kV coaxial gun at an energy of 3 keV and a beam current of 1 μA. The base pressure in the system was approximately 3×10^{-9} Pa. Most AES spectra were taken at room temperature, but spectra at the experimental temperature were also taken to ensure there was no difference. The samples were heated to the test temperature and maintained there for 30 minutes, and the spectra were then taken. The samples were then cooled to room temperature and spectra taken again. This procedure was repeated in 100° C increments from room temperature to a temperature of 1000° C.

Results and Discussion

In general, the Nb and the Ta did not seem to be significant in the dynamics of the surface composition as a function of temperature. The Nb was detected in the as-received and after-vacuum annealing (1000° C) conditions, but the surface was dominated by the Ti and Al reactions with the O, C, and S. The AES room-temperature surveys for the three materials showed the usual chemisorbed carbon- and oxygen-overlayer intensities, but no sulfur was detected.

Oxygen Variation

Figure 1 shows the surface variation of O concentration as a function of temperature from 20° C to 1000° C for pure Ti, α_2 aluminide, and γ aluminide. The high initial concentration of O results from adsorbed oxygen-bearing gases, such as H_2O, CO, and CO_2. The O on the surface of pure Ti was in the form of TiO_2 as indicated by the peak shapes and energy shifts of the Ti $L_3 M_{2,3}$ $M_{2,3}$ (383 eV), Ti $L_3 M_{2,3}$ V - shakeup (387 eV), Ti $L_3 M_{2,3}$ V (418 eV), and Ti L_3 VV (451 eV) transition peaks (9). The oxide was found to be relatively stable until T ≥ 400° C, where the surface concentration of the O dropped sharply to less than 5 percent (600° C). Since no desorption was observed, this suggests that the dissociation of TiO_2 proceeds by the dissolution of O into the Ti bulk. At T = 700° C, the O had completely disappeared from the surface (~ 3nm deep).

The α_2 and γ aluminides had the same initial O concentration, but compared with pure Ti, the oxygen seemed to decline in concentration almost immediately. The α_2 and γ aluminides had similar concentrations and slopes until T ≥ 700° C where a dramatic divergence in their respective concentrations was seen. The O intensity for the α_2 continued to decline to a final level of about 10 percent at 1000° C (6), but the intensity for the γ aluminide sharply increased to about 54 percent concentration at 900° C and then fell again to 34 percent at 1000° C. This behavior indicates that the γ aluminide surface concentration has changed in such a way that O diffuses from the bulk to form Al_2O_3. These dynamics were best observed by the low-energy variations (0 - 150 eV) shown in figure 2. The pure Ti spectra clearly show the 44-eV peak associated with TiO_2. This peak has been suggested by Shih and Jona (10) to be a cross transition between doubly ionized titanium and an

oxygen level. They observed a peak at 46 eV in the spectrum of clean Ti and a new peak at 40 eV in the spectrum of TiO_2. These discrepancies in peak energies may occur because they obtained the peak energies by double differentiation. The α_2 aluminide also shows a TiO_2 shoulder at room temperature, which became quite prominent at T = 500° C. At 700° C, an Al_xO_y suboxide + Al became apparent. As the temperature was further increased, the Al $L_{2,3}$ VV (68 eV) peak significantly increased accompanied by the obvious Al_xO_y shoulder. However, at no time was the TiO_2 lost, suggesting that the two oxides coexisted as patches or were layered. Figure 1 shows a substantial slowing of the O decline at 600° C for both α_2 and γ aluminides compared with pure Ti, possibly because the Al assists in retaining the O in the surface region (11, 12). The appearance of Al at 700° C in the α_2 aluminide also suggests a segregation of the Al to the surface through the TiO_2 with some exchange of the oxygen from the TiO_2 to form the Al_xO_y. This seems possible, since the diffusivity of Al through titanium aluminides is much greater than for Ti (13).

The γ aluminide, with its greater Al concentration, has an apparent Al_2O_3 intensity even at room temperature. The Al $L_{2,3}$ VV (68 eV) peak was first observed at 700° C, but the interatomic transition Al ($L_{2,3}$) O ($L_{2,3}$ $L_{3,3}$) peak at 54 eV which is Al_2O_3 became predominant at T ≥ 700° C. This is consistent with the oxygen increase for γ aluminide at T ~ 900° C shown in figure 1 and again represents a segregation of Al to the surface and loss of O from the TiO_2. At 1000° C, however, the O in the γ aluminide had substantially decreased because of the decomposition of Al_2O_3 and TiO_2 and the dissolution of O into the bulk, which left strong metallic Ti $M_{2,3}$ VV and Al $L_{2,3}$ VV peaks at 27 and 68 eV, respectively. Rough calculations of the room temperature oxide thickness (14) indicate that the TiO_2 formed on pure Ti appears to be the thickest (~ 3 nm), compared with the a_2 aluminide (~ 1.8 nm) and with the g aluminide (< 0.5 nm). This suggests that the varying oxide thickness formed on the titanium aluminides may be controlled by the Al content. Natural oxides on Al have been found to be approximately 1.8 nm compared with > 3 nm on TiO_2. These data are consistent with the fact that O can readily diffuse through TiO_2 to increase the oxide thickness, but O diffusion through Al_2O_3 is so slow that it limits oxide growth.

Carbon Variation

Figure 3 shows the variation in the C concentration as a function of temperature for pure Ti and the α_2 and γ aluminides. The increase in intensity in the 300-400° C range is primarily an overlayer effect from the decomposition of the TiO_2 and the dissolution of the oxygen. In pure Ti, the C is completely dissolved at 700° C, but in the α_2 and γ aluminide, there is still some residual concentration (~ 3 percent) after 1000° C. The C concentration from the γ aluminide was observed to be as high as 21 percent in the 600-700° C range. The retention of the C also appears to be connected with the Al content, perhaps associated with a lower C diffusivity through the higher alloy aluminides. Figure 4 shows a variation of the carbide percentage on pure Ti and the γ aluminide as a function of temperature. These values were calculated by using the asymmetry ratio of the Auger line shape of the carbide reported by Baldwin and co-workers (15). The carbide percentage for the α_2 aluminide was not presented because it was basically amorphous up to 500° C and dissolved so rapidly at T > 500° C that carbide formation was not apparent. The formation of the carbide seems to be related to the availability of free Ti in the sample, since the carbide forms at a rate that is connected with the absence of oxygen. (Compare figure 4 with figure 1.) This may be a reasonable conclusion, since the free energy of formation of TiO_2 at 500° C (ΔG = - 795 kJ/mole) is much smaller than TiC (ΔG = - 184 kJ/mole) (16). The dissociation temperature of the carbide on the γ aluminide (700° C) is higher than on the pure Ti (500° C) because of, as mentioned

previously, a possible decrease in C diffusivity through higher Al content alloys.

Sulfur Variation

Although S is not a significant bulk impurity (< 1 ppm), segregation up the grain boundaries and defects to the surface can make it appear substantial. Figure 5 shows the variation of S concentration as a function of temperature for the pure Ti and the α_2 and γ aluminides. The segregation of the S to the surface appears to be strongly inhibited by the species (i.e., carbon or oxygen) interacting with Ti. For example, the three S curves are almost exactly the inverse of the O curves shown in figure 1, which indicates that the S will not segregate until the O is substantially depleted from the surface region. To a lesser extent, the same appears to be true for S segregation following the C dissolution, since C closely follows the O dissolution. Further, no peak shape variation or energy shift was observed for the S LVV (152 eV) transition, which suggests that the S surface bond is a tenuous one. The S intensity increased dramatically at $T \geq 500°$ C for the pure Ti and somewhat slower for the α_2 aluminide ($T \geq 600°$ C), but since the γ aluminide retained a rather significant oxygen level at high temperature, the detected S never increased beyond 10 percent, even at 1000° C. The S was found to be easily removed from the surface, by short-term Ar ion sputtering or by in situ O exposure, which further confirms that the S was weakly bound (6).

Conclusions

1. At room temperature, TiO_2 was observed as the predominant surface oxide for pure Ti and the α_2 and γ aluminides. At 400° C, the TiO_2 surface on pure Ti decomposed in UHV; at 500° C, the TiO_2 and Ti peaks split; and at 600° C only metallic peaks were observed.
2. At 700° C, the α_2 aluminide shows the formation of some Al_xO_y + Al, presumably from Al diffusing through the TiO_2 layer to the surface. As the temperature increased, the metallic Al peak became more and more prominent, suggesting an Al overlayer or Al patches.
3. The γ aluminide shows both TiO_2 and Al_2O_3 at room temperature, reflecting the higher concentration of Al compared with α_2 aluminide. At 700° C, surface Al was detected, which attracted oxygen to the surface to become Al_2O_3, probably as an overlayer on TiO_2. At 1000° C, predominantly metallic Al and Ti were observed, since the oxygen had dissolved into the bulk. (A small TiO_2 signal was still retained.)
4. Subsequent to the dissolution of oxygen into the bulk, molecular C was converted to 100 percent TiC at 500° C for pure Ti and at 700° C for γ aluminide. Dissolution of C into the bulk was so rapid for the α_2 aluminide, no significant carbide formation was observed.
5. The amount of S segregated to the surface was in descending order, pure Ti > α_2 aluminide > γ aluminide, presumably because the higher Al content retained proportionally more O, restricting the available sites to sulfur.

References

1. H. A. Lipsitt, Titanium Aluminides - An Overview, In High Temperature-Ordered Intermetallic Alloys, MRS Symposia Proceedings, edited by C. C. Koch, C. T. Liu, and N. S. Stoloff, p. 351 Material Research Society, Pittsburgh (1985).
2. M. Kabbaj, A. Galerie, and M. Caillet, J. Less Common Metals 108, 1 (1985).

3. S. M. L. Sastry and H. A. Lipsitt, Ti'80, Science and Technology, edited by H. Kimura and O. Izumi, p. 1231, TMS-AIME, Warrendale, Pa (1980).
4. D. Banerjee, T. K. Nandy, and A. K. Gogia, Scripta Metall. 21, 597 (1987).
5. N. S. Chowdary, H. C. Graham, and J. W. Hinze, Oxidation Behavior of Titanium Aluminides, in proceedings of the symposium on Properties of High-Temperature Alloys, edited by Z. A. Foroulis and F. S. Pettit, p. 668, Electrochemical Society, Princeton, New Jersey (1977).
6. W. S. Lee, S. N. Sankaran, R. A. Outlaw, and R. K. Clark, J. Electrochem. Soc. 137, 1194 (1990).
7. S. N. Sankaran, R. A. Outlaw, and R. K. Clark, "Surface Effects on Hydrogen Permeation Through Ti-14Al-21Nb Alloys." To be published as NASA Technical Publication.
8. D. S. Shih, G. K. Scarr, and G. E. Wasielewski, Scripta Metall. 23, 973 (1989).
9. J. S. Solomon and W. L. Baun, Surf. Sci. 51, 228 (1975).
10. H. D. Shih and F. Jona, Appl. Phys. 12, 311 (1977).
11. J. Subrahmanyam, J. Mater. Sci. 23, 1906 (1988).
12. Y. Umakoshi, M. Yamaguchi, T. Sakagami, and T. Yamane, J. Mater. Sci. 24, 1599 (1988).
13. J. Tardy and K. N. Tu, Phys. Rev. B, 32, 1070 (1985).
14. P. H. Holloway, J. Vac. Sci. Technol., 12, 1418 (1975).
15. D. A. Baldwin, B. D. Sartwell, and I. L. Singer, Appl. Surf. Sci. 25, 364 (1986).
16. C. E. Wicks and F. E. Block, in Bull. U. S. Bur. Mines, No. 605, (1963).

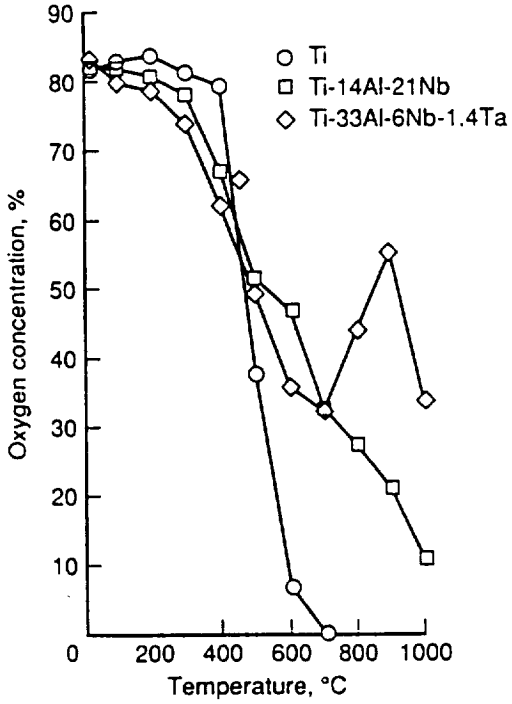

FIG. 1 Oxygen concentration as a function of temperature for Ti and the α_2, γ aluminides.

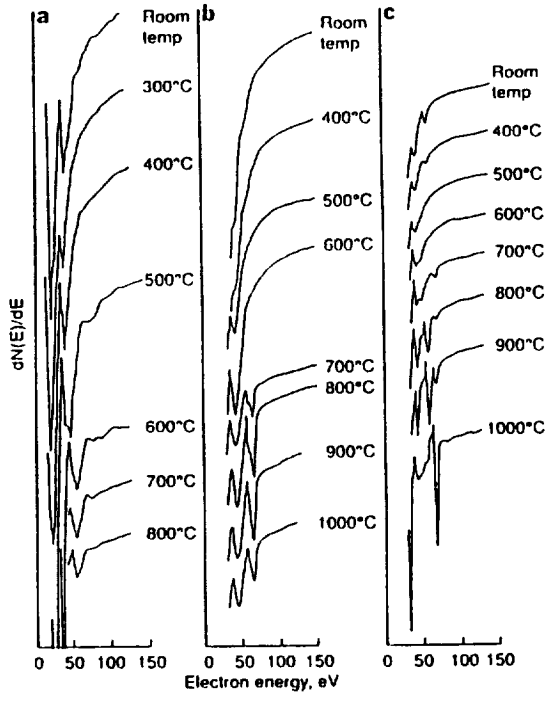

FIG. 2 Low energy (0 - 150 eV) AES surveys as a function of temperature for (a) Ti, (b) α_2 aluminide, and (c) γ aluminide.

FIG. 3 Carbon concentration as a function of temperature for Ti and the α_2, γ aluminides.

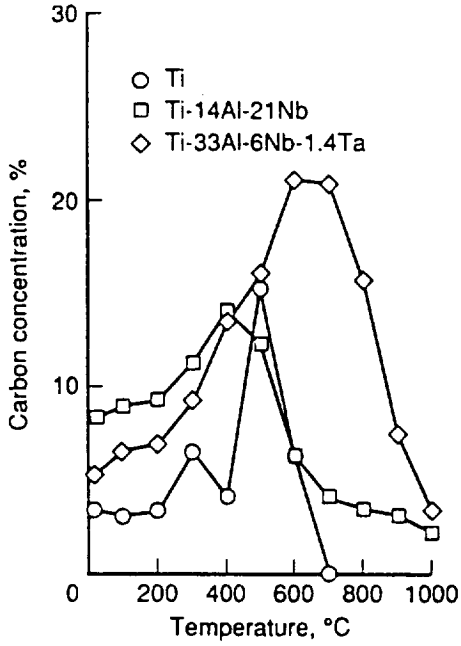

FIG. 4 Carbide formation as a function of temperature for Ti and γ aluminide. Auger peak shapes for each point are also shown.

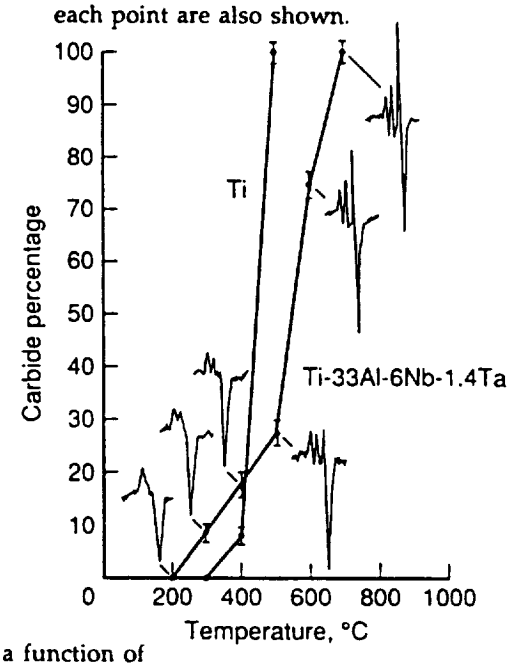

FIG. 5 Sulfur concentration as a function of temperature for Ti and the α_2, γ aluminides.

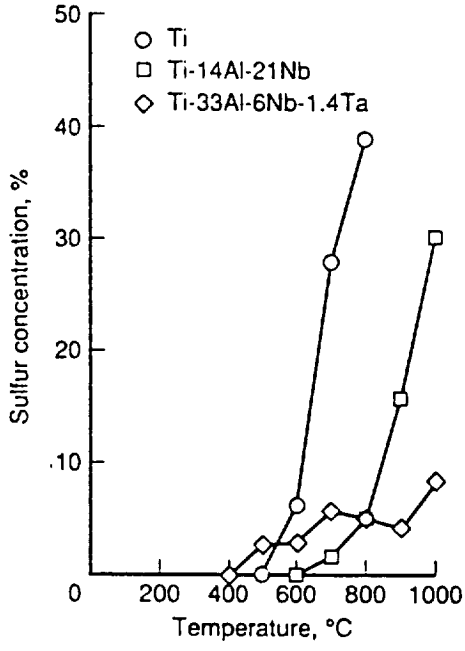

Applied Surface Science 47 (1991) 91–98
North-Holland

Auger electron intensity variations in oxygen-charged silver

W.S. Lee
Department of Physics, Hampton University, Hampton, VA 23668, USA

R.A. Outlaw
NASA Langley Research Center, Hampton, VA 23665-5225, USA

G.B. Hoflund and M.R. Davidson
University of Florida, Gainsville, FL 32611, USA

Received 11 January 1990; accepted for publication 16 July 1990

Auger intensity variations over an oxygen-charged polycrystalline silver surface have been observed by studies of Auger images and line scans of selected adjacent grains which were determined to be the (421) and (221) orientations. The observed contrast (M_4VV transition) between the grains is produced by the variation in the detected Auger electrons caused by the different directions (interatomic direction) of forward focusing in each grain. The contrast produced by the Ag Auger electrons was found to be strongly dependent on the surface order of the grains, but that of the O Auger electrons was not, presumably because the atoms were randomly distributed throughout the Ag surface or subsurface. The contrast observed between the grains at the lower Auger energies (N_1VV and $N_1N_{2,3}$V transitions) appeared to be produced by constructive interference from multiple scattering. The $N_1N_{2,3}$V electrons at 29 eV, for example, gave higher contrast than that of the N_1VV transition at 78 eV.

1. Introduction

In Auger electron spectroscopy (AES) the diffraction of both the incident electrons used for the initial excitation and the emitted Auger electrons can provide contrast effects which are scientifically meaningful. Auger electrons with a few hundred eV or higher are strongly forward focused by atoms in their path, especially by atoms near the electron source. Further, Auger electrons in this energy range are diffracted such that they correspond to interatomic directions, which suggest that final-state scattering is dominant and that the nature of the emission process is not a contributing factor. As a result of these mechanisms, forward focusing of medium-energy Auger electrons (200–1000 eV) has emerged as a very useful tool for studying epitaxial growth, interfaces, and surface structural determination [1–13]. At lower energies ($E_k \leq 300$ eV) forward focusing is less significant and cannot be directly related to interatomic directions due to the greater effect of multiple scattering [1,3,4,9]. Assuming that in standard AES the focusing effects are induced by a plane wave of incident electrons, these effects might be amplified in certain atomic directions and give rise to a layer-dependent Auger electron yield, besides the conventional mean-free-path consideration. Indeed, several authors have investigated the effects of diffraction of the incident electron. Chambers and co-workers [14] have investigated the role that the incident beam direction might play in producing anisotropies in angle-resolved Auger electron emission and found that Pd MNN (330 eV) Auger emission exhibits maxima along low-index interatomic directions, and that these effects are independent of the angle of incidence. Gomoyunova and co-workers [15] have observed that intensity enhancement of elastically backscattered primary electrons along

0169-4332/91/$03.50

low-index interatomic directions is the same as that observed for Auger electrons. Recently, Van Hove and co-workers [16,17] have explored the effect of the incident electrons scattered into the crystal by considering a plane wave incident on a chain of atoms (e.g., the [100] direction in the (100) orientation) and observed that amplification and focusing enhancements occur prominently. Amplification occurs when the incident direction is about 10° away from the chain direction. The scattered wave can add onto the direct incident wave reaching deeper atoms, and this results in more electron flux than just from the top-most surface atoms. Otherwise, focusing enhancement occurs when the incident direction is within the peak half-width from the chain axis direction (about 5°). The second atom down the chain receives the largest electron flux due to focusing by the first atom, while defocusing prevents the third and deeper atoms from being exposed as much to the electrons. However, forward focusing of the incident electrons is relatively less important to that of emitted Auger electrons because an incident plane wave undergoes many more interferences than does an outgoing Auger-electron spherical wave [16].

In this paper, our objectives were to explore the relative intensity of the silver and oxygen Auger peaks obtained from different large grains of oxygen-charged polycrystalline silver, to investigate which Auger transition energies of silver are subject to forward focusing, and to examine the effect of oxygen atoms located on the Ag surface or subsurface. We have intentionally chosen two adjacent, crystallographically similar grains, the (421) and the (221), in oxygen-charged polycrystalline silver in order to observe the relative sensitivity of the diffraction effects.

2. Experimental

The experimental system is comprised of a standard ultra-high vacuum (UHV) work chamber pumped by a 150 ℓ/s ion pump and a titanium sublimation pump (base pressure is around 2×10^{-12} Torr). The system is equipped with a four-grid optics system for low-energy electron diffraction (LEED), a 10 kV cylindrical mirror analyzer for AES with an electron beam size of approximately 2 μm, a quadrupole mass spectrometer for residual gas analysis, and several ion and electron guns.

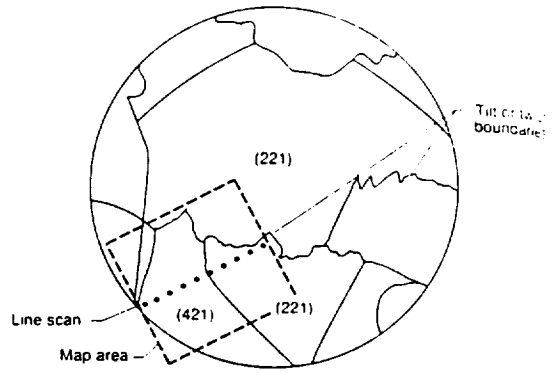

Fig. 1. Tracing of the grain boundaries of the polycrystalline silver sample. Dashed region encloses area studied and dotted line is path of line scans.

The sample (0.999999+vacuum melted Ag) used in this work was spark-machined from large-grain silver into the shape of a 5 mm square, 0.254 mm thick coupon. The grain sizes were found to be in the range of 1–5 mm diameter. The grains of the sample selected for study were analyzed by Laue back-diffraction techniques to determine their orientation. A metal mask was used to reduce the size of the Cu Kα beam to be less than 0.5 mm. The grain size was on average about 2 mm, so the beam was completely intercepted by each individual grain. The sample was positioned by a vernier stage to the selected grains of interest where the diffraction pattern was captured on film. Fig. 1 shows a tracing of the grain structure in the region studied which are the (421) and (221) grains. The (221) grain is only about 15° off of the (111) pole. The grain boundary at the top of the tracing is probably a tilt or twist boundary. The (421) grain appears to be rotated about 90° from the [$\bar{1}$10] direction of the (221). The angle between the poles of these two orientations was approximately 19°. The sample was mechanically and chemically polished, ultrasonically cleaned in detergent, ultrasonically rinsed in deionized water, hot air dried, and then immediately installed into

the sample introduction/preparation chamber. The sample was initially degassed at 600 °C for 2 h, cooled to room temperature, and then backfilled with oxygen to 100 Torr and reheated to 600 °C for 2 h. The sample temperature of 600 °C was selected in order to maximize the solubility of oxygen in silver because the desorption of oxygen from the silver membrane (vacuum on both sides) has been observed to occur at approximately 600 °C [18]. After charging the silver with oxygen, the sample was then transferred into the UHV analysis chamber for study.

3. Results and discussion

An AES analysis of the oxygen-charged silver in 100 Torr oxygen at 600 °C for 2 h showed some small concentration of carbon and oxygen. After a brief argon ion bombardment, a representative Auger spectrum of the clean oxygen-charged silver is as shown in fig. 2. Note here that the 351 eV and the 356 eV peaks are not resolved because a modulation of 10 V was used to sufficiently increase the sensitivity so that the oxygen peak at 503 eV could be detected. The inset shows the Ag prior to oxygen charging and after Ar ion sputtering (modulation 2 V) where the 351 and 356 eV peaks are clearly resolved. The oxygen-to-silver $M_{4,5}VV$ (356 eV) ratio was determined to be approximately 4%, which is in good agreement with the results of Rovida and Pratesi [19,20]. They found a ratio of up to 4% on both Ag(111) and Ag(110) single-crystal surfaces.

Fig. 3 shows Auger images and line scans of Ag and O after a brief cleaning by argon ion bombardment (figs. 3a and 3b) and after a subsequent anneal at 470°C at 5×10^{-11} Torr for 30 min (figs. 3c and 3d). Fig. 3a shows that there is some weak Ag contrast and intensity variation between grains of the sample. Fig. 3b, however, which represents the dissolved oxygen image and line scan, does not show any significant contrast. After heating the sample at 470 °C at 5×10^{-11} Torr for 30 min, the damage incurred by ion bombardment was annealed out, and the contrast shown in fig. 3c was correspondingly greater. (Compare fig. 3c with fig. 3a.) The anneal, however, did not significantly improve the dissolved oxygen contrast between the grains (fig. 3d) but did appear to concentrate more oxygen at the surface. These results indicate that the observed contrast strongly depends on the surface order of the grains. The source of the contrast is quite probably the variation in the Auger electrons caused by the different directions (interatomic direction) of forward focusing in each grain. This diffraction of the outgoing electrons is primarily caused by the overlying lattice atoms to a depth of about 4 atomic layers [2,11,12]. Multiple scattering also plays an important role in preventing intensity enhancements in the emission from deeper than the top few layers (i.e., subsequent layers are defocusing) [1,2,11,12,21,22]. The lack of O(KLL) contrast in the same two grains may be because oxygen atoms are randomly distributed throughout the Ag surface or subsurface and are not in positions aligned with chains of Ag atoms [13,23]. Oxygen in saturated silver has been observed in LEED experiments to occupy no particular order [24]. It is assumed that most of the oxygen atoms

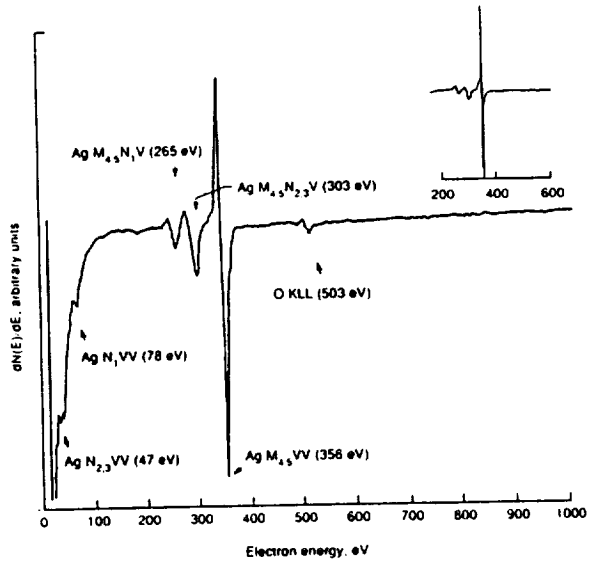

Fig. 2. Auger spectrum of the Ag sample cleaned by Ar ion bombardment after charging with oxygen at 100 Torr and at 600 °C for 2 h; normal incidence; primary electron beam energy $E_p = 2000$ eV; primary beam current $I_p = 1.3$ μA; modulation voltage 10 V. Inset shows primary Ag transitions before oxygen charging; modulation voltage 2 V.

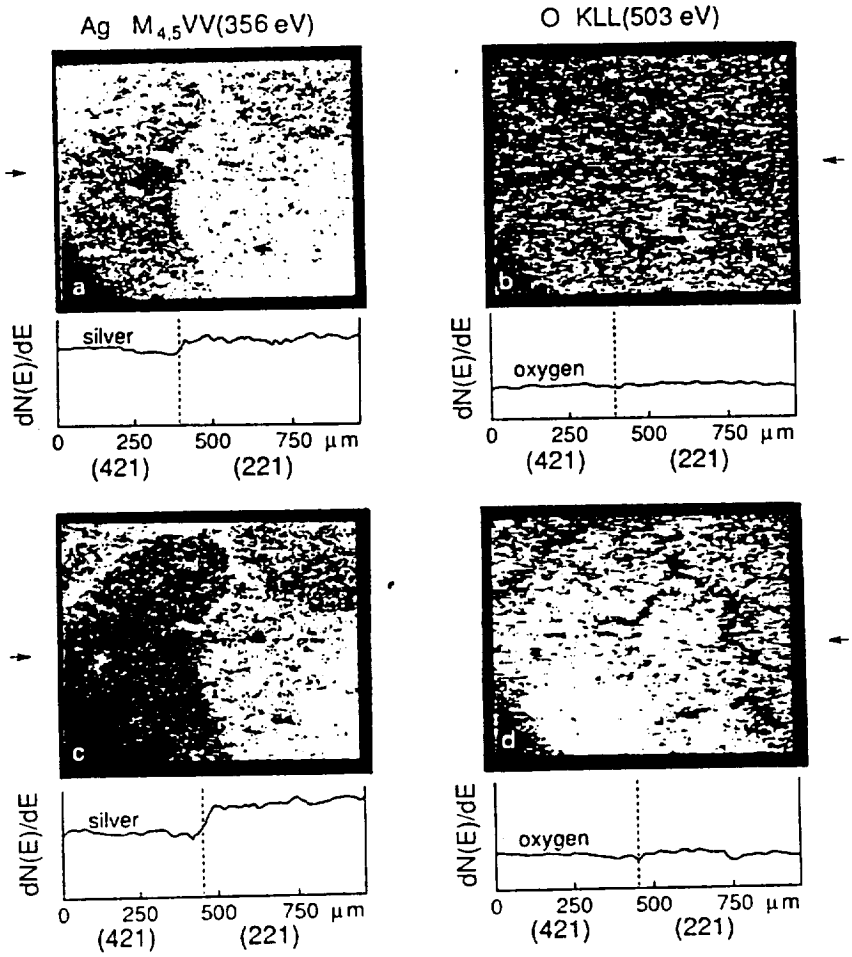

Fig. 3. Auger images and line scans of Ag $M_{4,5}VV$ (356 eV) and O KLL (503 eV). Arrows indicate the position of line scans. Dashed lines represent position of grain boundary. Normal incidence; $E_p = 3000$ eV; $I_p = 0.1$ μA; modulation 10 V: (a) Ag $M_{4,5}VV$ after cleaning by ion bombardment; (b) O KLL after cleaning by ion bombardment; (c) Ag $M_{4,5}VV$ after heating at 470 °C in UHV for 30 min; (d) O KLL after heating at 470 °C in UHV for 30 min.

are located in the octahedral interstitial sites of the Ag because the radius of the octahedral sites ($r_{oct} = 0.598$ Å) is much larger than that of the tetrahedral sites ($r_{tet} = 0.325$ Å) of the fcc structure, and is also comparable to the single-bond covalent radius of the oxygen atoms ($r_{oxy} \approx 0.66$ Å). These interstitial regions are also affected by surface relaxation, which occurs in the form of expansions and contractions that do not change the two-dimensional lattice but do change in the z-direction near the surface [25–30]. The varying layer spacing normal to the surface exhibits a damped oscillatory size distribution. Most oxygen atoms will probably be located between the second and third layers because the spacing is generally expanded, whereas the spacing between the first and second layers is generally contracted. Oxygen atoms have also been observed by Van Hove and co-workers to randomly occupy octahedral sites below the first and second layers of Mg(0001), causing a small expansion of about 0.1 Å [13]. Fig. 4 shows a plot of the O(KLL) to

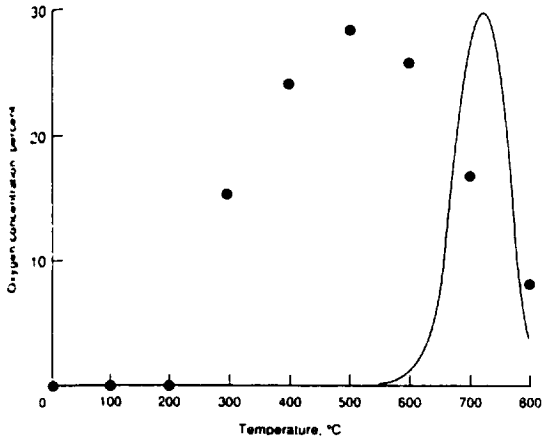

Fig. 4. O(KLL) to Ag $M_{4,5}VV$ peak ratio plotted as a function of annealing temperature over the range 20 to 800 °C. Note the aggregation of oxygen to the near surface peak at 500 °C. Continuous line indicates vacuum desorption signal.

Ag($M_{4,5}VV$) ratio plotted as a function of annealing temperature (20 to 800 °C, 30 min at each temperature). Clearly, the aggregation of the oxygen to the Ag surface or subsurface increased up to about 500 °C and then began to decrease because of desorption (solid line). Even though surface aggregation is quite apparent, the lack of contrast suggests no ordering of the oxygen occurred. The heat of formation of bulk Ag_2O has been reported to be ~ 14.5 kcal/mol O_2 as compared to the heat of adsorption of oxygen on Ag which is ~ 42.4 kcal/mol O_2, which suggests that the oxide is much less stable than the chemisorbed state [31] and that the thermal energy of the anneals may have been sufficient to inhibit ordering, especially since the oxide was so tenuous. It therefore appears that the surface and subsurface oxygen were completely random and not aligned with the Ag lattice atoms.

Fig. 5 shows the variation of the O(KLL) peak to the Ag($M_{4,5}VV$) peak ratio for the grains presented in fig. 3. The oxygen-to-silver ratio obtained after cleaning by ion bombardment is around 3.7% with no significant change of ratio between the different grains (fig. 5, solid circles). The oxygen-to-silver ratio obtained after heating at 470 °C in UHV for 30 min, however, is different, 10.8% in the (421) grain and 9.1% in the (221) grain (fig. 4, open circles). This difference comes

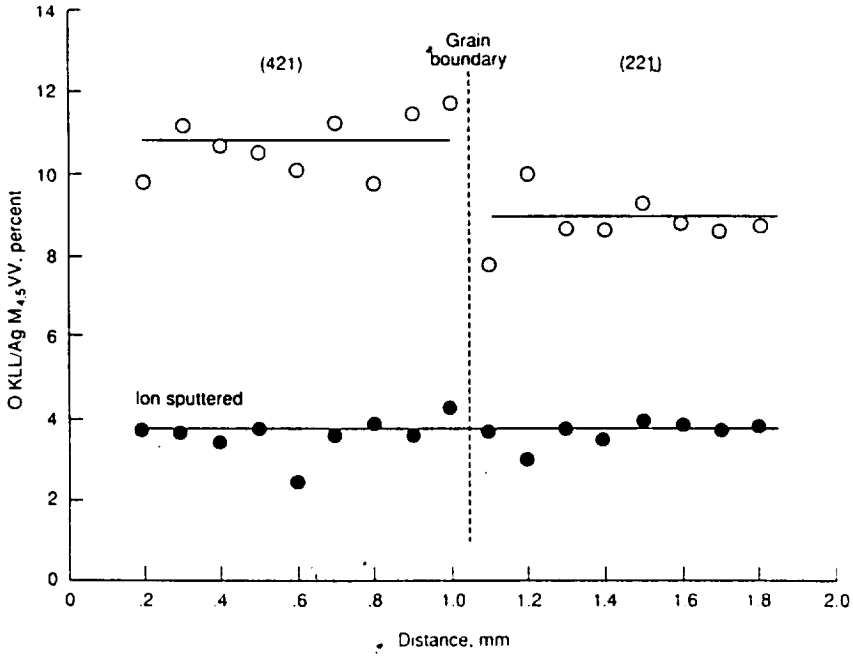

Fig. 5. Variation of oxygen-to-silver ($M_{4,5}VV$) peak ratio with different grains. Solid circles indicate ratio after cleaning by ion bombardment; open circles indicate ratio after heating at 470 °C in UHV for 30 min.

from the intensity variation of the Ag($M_{4,5}$VV) peak with different ordered grains, and the fact that the oxygen Auger intensity did not change. Further, this result also indicates that the intensity variation of the Ag($M_{4,5}$VV) peak is independent of the amount of oxygen near the surface.

Fig. 6 shows images and line scans of different Auger transition energies of silver after heating

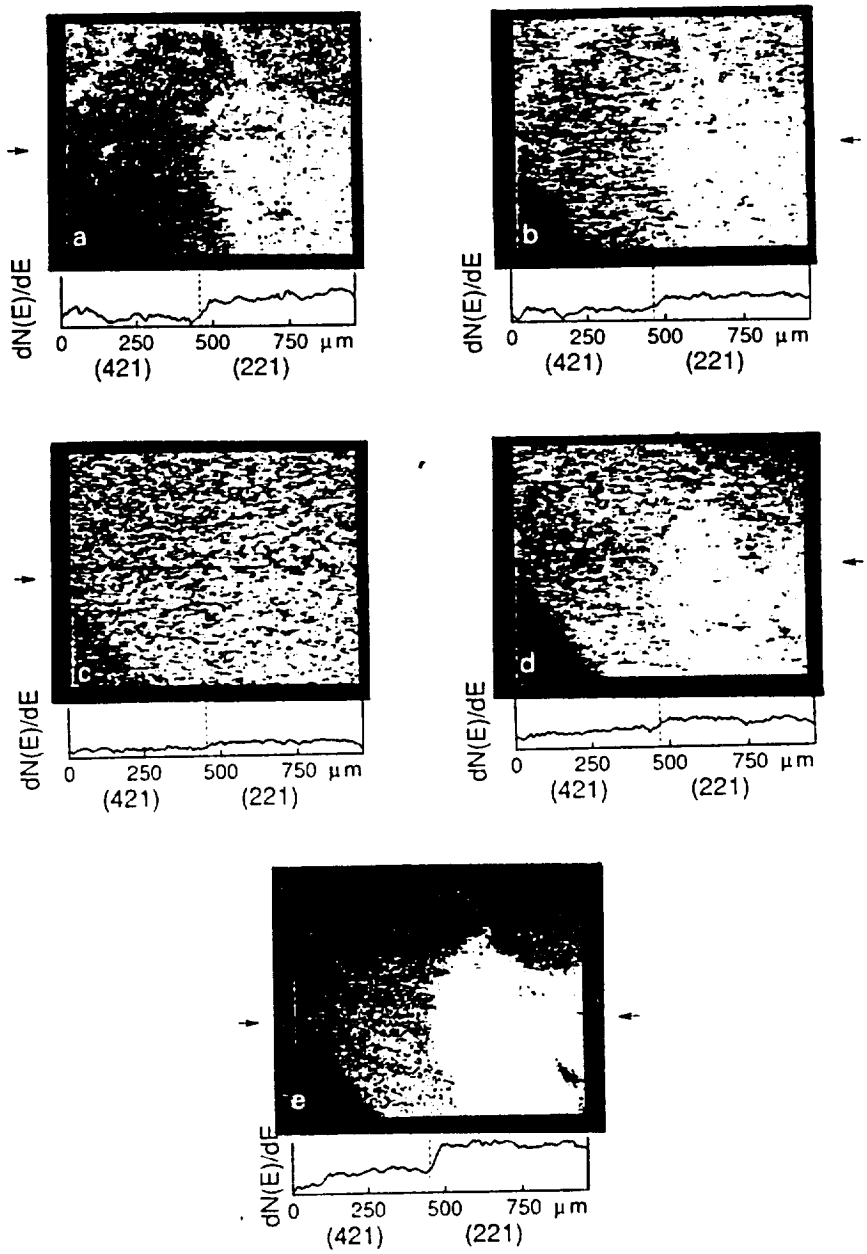

Fig. 6. Auger images and line scans of the different Ag Auger transitions. Arrows indicate the position of line scan. Dashed lines represent position of grain boundary. Normal incidence; E_p = 3000 eV; I_p = 1.0 µA; modulation 10 V. (a) Ag $M_{4,5}$VV (356 eV); (b) Ag $M_{4,5}N_{2,3}$V (303 eV); (c) Ag $M_{4,5}N_1$V (265 eV); (d) Ag N_1VV (78 eV); (e) Ag $N_1N_{2,3}$V (27 eV).

the sample at 470°C in UHV for 30 min. The contrast of the Auger images of silver on different grains shows a strong dependence with transition energy. The highest contrasts are shown in figs. 6a and 6e, the $M_{4,5}VV$ (356 eV) and $N_1N_{2,3}V$ (27 eV) transitions, respectively. The lowest contrast is shown fig. 6c, the $M_{4,5}N_1V$ (265 eV) transition. Moderate contrasts are shown in figs. 6b and 6d, the $M_{4,5}N_{2,3}V$ (303 eV) and N_1VV (78 eV) transitions, respectively. In general, the enhancement of the forward focusing increases as the electron kinetic energy increases, while the half-width of the peak decreases [11]. Although Poon and Tong [11] have suggested that the energy at which forward focusing starts depends on details of the atom potential (e.g., Cu starts at energies above 60 eV), it is evident that previous attempts to use intermediate-energy electrons (~ 300 eV) for structural studies showed substantially less diffraction fine structure [1]. Further, the electron–atom scattering factors weaken and broaden in the forward direction and side and backscattering lobes begin to develop [9].

Chambers and co-workers have shown that low kinetic energy electrons can be a useful tool for studying the early stages of epitaxial growth in bimetallic interfaces of Ag/Pd (001) [4]. Although polar-angle intensity profiles associated with the Pd MNN (326 eV) and the Ag MNN (351 eV) Auger peaks as a function of Ag coverage showed good agreement with local diffraction-induced maxima along low-index directions resulting from forward focusing, it is evident that the intensity enhancement of the lower kinetic energy peak (Pd MNN) is less than that of the higher kinetic energy peak (Ag MNN) because of the zeroth-order forward scattering in the [101] direction.

In figs. 6a–6c, it is found that the lower the Ag Auger electron energy, the less the contrast of the Auger images on different grains. These results are in good agreement with previous results [1,4,9,11]. The Ag $M_{4,5}N_1V$ (265 eV) transition exhibits the least contrast and can be explained by the fact that forward focusing at this electron energy along low-index directions is limited because of multiple scattering, i.e., the Auger electron emerges without a strong preference for a particular direction.

Generally, at low kinetic energies, say below 100 eV, the multiple scattering by a single atom is unfocused [17]. This result does not mean isotropic Auger emission, but means that these peaks do not exactly correspond to interatomic axes. Actually forward focusing is due to the individual atomic scattering amplitude: a spherical wave representing an electron scatters primarily within a forward cone which has a half-width of about 10° [13]. Indeed, marked anisotropic Auger emission in the energy range 45–70 eV has been measured for the Fe [32], Cu [33], Ni [34], Ag [35], and Al [36] single-crystal surfaces. All of these anisotropic peaks did not relate to interatomic axes, but the intensity variation was significant with polar and azimuthal angles.

In figs. 6d and 6e, which represent the 78 to 27 eV transitions, the contrast at 27 eV is higher. This may be explained by interference peaks due to combinations of paths that interfere to produce constructive maxima in the distributions at various polar and azimuthal angles. The longer de Broglie wavelength at these energies also results in a greater degree of constructive and destructive interference by multiple scattering.

4. Conclusions

(1) The marked contrast in Auger images between adjacent grains of Ag, specifically the (421) and (221) orientations, is because of the different interatomic direction of forward focusing of Auger electrons which originated around two to four atomic layers into the surface. Intensity enhancement of the Auger electrons depends on the degree of surface order of the grain. Auger electrons which originated from randomly distributed oxygen in the surface or subsurface showed no contrast because the oxygen atoms are not in positions aligned with chains of Ag atoms and have no intrinsic order. The intensity variation of the Ag $M_{4,5}VV$ peak is independent of the amount of randomly located oxygen near the surface.

(2) The contrast observed in Auger images between the different Ag transition energies is primarily due to marked anisotropic emission. Specifically, the contrast between the 356 and the 265 eV transitions is due to the diminishing forward

focusing and increased multiple scattering at the lower energy. The contrast improves again at lower transition energies (78 and 27 eV) when constructive interference produces maxima at various polar and azimuthal angles.

(3) The $AgM_{4,5}N_1V$ (265 eV) electrons appear to be the lower energy limit of forward focusing that corresponds to the interatomic axes.

References

[1] W.F. Egelhoff, Jr., Phys. Rev. B 30 (1984) 1052.
[2] W.F. Egelhoff, Jr., Phys. Rev. Lett. 59 (1987) 559.
[3] S.A. Chambers and L.W. Swanson, Surf. Sci. 131 (1983) 385.
[4] S.A. Chambers, S.B. Anderson and J.H. Weaver, Phys. Rev. B 32 (1985) 4872.
[5] S.A. Chambers, S.B. Anderson and J.H. Weaver, Phys. Rev. B 32 (1985) 581.
[6] S.A. Chambers, H. W. Chen, I.M. Vitomirov, S.B. Anderson and J.H. Weaver, Phys. Rev. B 33 (1986) 8810.
[7] S.A. Chambers, S.B. Anderson, H.W. Chen and J.H. Weaver, Phys. Rev. B 35 (1987) 2592.
[8] P.J. Orders, R.E. Connelly, N.F.T. Hall and C.S. Fadley, Phys. Rev. B 24 (1981) 6163.
[9] E.L. Bullock and C.S. Fadley, Phys. Rev. B 31 (1985) 1212.
[10] E.L. Bullock, C.S. Fadley and P.J. Orders, Phys. Rev. B 28 (1983) 4867.
[11] H.C. Poon and S.Y. Tong, Phys. Rev. B 30 (1984) 6211.
[12] S.Y. Tong, H.C. Poon and D.R. Snider, Phys. Rev. B 32 (1985) 2096.
[13] H. Cronacher, K. Heinz, K. Müller, M.L. Xu and M.A. Van Hove, Surf. Sci. 209 (1989) 387.
[14] S.A. Chambers, H.W. Chen, S.B. Anderson and J.H. Weaver, Phys. Rev. B 34 (1986) 3055.
[15] M.V. Gomoyunova, I.I. Pronin and I.A. Shmulevitch, Surf. Sci. 139 (1984) 443.
[16] M.L. Xu and M.A. Van Hove, Surf. Sci. 207 (1989) 215.
[17] M.L. Xu, J.J. Barton and M.A. Van Hove, Phys. Rev. B 39 (1989) 8275.
[18] R.A. Outlaw, S.N. Sankaran, G.B. Hoflund and M.R Davidson, J. Mater. Res. 3 (1988) 1378.
[19] G. Rovida and F. Pratesi, Surf. Sci. 43 (1974) 230.
[20] G. Rovida and F. Pratesi, Surf. Sci. 52 (1975) 542.
[21] S. Kono, C.S. Fadley, N.F.T. Hall and Z. Hussain, Phys. Rev. Lett. 41 (1978) 117.
[22] S. Kono, C.S. Fadley, N.F.T. Hall and Z. Hussain, Phys. Rev. B 22 (1980) 6085.
[23] C.S. Fadley and S.A.L. Bergström, Phys. Lett. A 35 (1971) 375.
[24] E. Zanazzi, M. Maglietta, U. Bardi and F. Jona, J. Vac. Sci. Technol. 1 (1983) 7.
[25] J.R. Smith and A. Banerjea, J. Vac. Sci. Technol. A 6 (1988) 812.
[26] S.M. Yalisove and W.R. Graham, J. Vac. Sci. Technol. A 6 (1988) 588.
[27] S.M. Foiles, M.I. Baskes and M.S. Daw, Phys. Rev. B 33 (1986) 7983.
[28] P. Jiang, P.M. Marcus and F. Jona, Solid State Commun. 59 (1986) 275.
[29] Y. Kuk and L.C. Feldman, Phys. Rev. B 30 (1984) 5811.
[30] J. Sokolov, F. Jona and P.M. Marcus, Solid State Commun. 49 (1984) 307.
[31] C.T. Campbell, Surf. Sci. 157 (1985) 43.
[32] T. Matsudaira, M. Watanabe and M. Onchi, Jpn. J. Appl. Phys. Suppl. 2, Pt. 2 (1974) 181.
[33] L. McDonnell, D.P. Woodruff and B.W. Holland, Surf. Sci. 51 (1975) 249.
[34] S.P. Weeks and A. Liebsch, Surf. Sci. 62 (1977) 197.
[35] T. Matsudaira and M. Onchi, Surf. Sci. 74 (1978) 684.
[36] G. Allié, E. Blanc and D. Dufayard, Surf. Sci. 57 (1976) 293.